Volatile Cycling of H2O, CO2, F, and Cl in the HIMU Mantle: A New Window Provided by Melt Inclusions from Oceanic Hot Spot Lavas at Mangaia, Cook Islands

Rita A. Cabral

Matthew G. Jackson

Kenneth T. Koga

Estelle F. Rose-Koga

Erik H. Hauri

See next page for additional authors

Follow this and additional works at: https://digitalcommons.uri.edu/gsofacpubs

Citation/Publisher Attribution

Volatile Cycling of H2O, CO2, F, and Cl in the HIMU Mantle: A New Window Provided by Melt Inclusions from Oceanic Hot Spot Lavas at Mangaia, Cook Islands
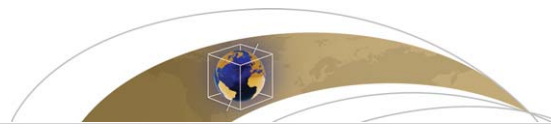
Publisher Statement

Authors

Rita A. Cabral, Matthew G. Jackson, Kenneth T. Koga, Estelle F. Rose-Koga, Erik H. Hauri, Martin J. Whitehouse, Allison A. Price, James M.D. Day, Nobumichi Shimizu, and Katherine A. Kelley

Terms of Use

Volatile cycling of H_2O, CO_2, F, and Cl in the HIMU mantle: A new window provided by melt inclusions from oceanic hot spot lavas at Mangaia, Cook Islands

Rita A. Cabral[1], Matthew G. Jackson[2], Kenneth T. Koga[3], Estelle F. Rose-Koga[3], Erik H. Hauri[4], Martin J. Whitehouse[5], Allison A. Price[2], James M. D. Day[6], Nobumichi Shimizu[7], and Katherine A. Kelley[8]

[1]Department of Earth and Environment, Boston University, Boston, Massachusetts, USA, [2]Department of Earth Science, University of California Santa Barbara, Santa Barbara, California, USA, [3]Université Blaise Pascal - CNRS - IRD, Laboratoire Magmas et Volcans, OPGC, Clermont-Ferrand, France, [4]Department of Terrestrial Magnetism, Carnegie Institution of Washington, Washington, DC, USA, [5]Department of Geosciences, Swedish Museum of Natural History, Stockholm, Sweden, [6]Geosciences Research Division, Scripps Institution of Oceanography, La Jolla, California, USA, [7]Department of Geology and Geophysics, Woods Hole Oceanographic Institution, Woods Hole, Massachusetts, USA, [8]Graduate School of Oceanography, University of Rhode Island, Narragansett, Rhode Island, USA

Abstract Mangaia hosts the most radiogenic Pb-isotopic compositions observed in ocean island basalts and represents the HIMU (high $\mu = {}^{238}U/{}^{204}Pb$) mantle end-member, thought to result from recycled oceanic crust. Complete geochemical characterization of the HIMU mantle end-member has been inhibited due to a lack of deep submarine glass samples from HIMU localities. We homogenized olivine-hosted melt inclusions separated from Mangaia lavas and the resulting glassy inclusions made possible the first volatile abundances to be obtained from the HIMU mantle end-member. We also report major and trace element abundances and Pb-isotopic ratios on the inclusions, which have HIMU isotopic fingerprints. We evaluate the samples for processes that could modify the volatile and trace element abundances postmantle melting, including diffusive Fe and H_2O loss, degassing, and assimilation. H_2O/Ce ratios vary from 119 to 245 in the most pristine Mangaia inclusions; excluding an inclusion that shows evidence for assimilation, the primary magmatic H_2O/Ce ratios vary up to ∼200, and are consistent with significant dehydration of oceanic crust during subduction and long-term storage in the mantle. CO_2 concentrations range up to 2346 ppm CO_2 in the inclusions. Relatively high CO_2 in the inclusions, combined with previous observations of carbonate blebs in other Mangaia melt inclusions, highlight the importance of CO_2 for the generation of the HIMU mantle. F/Nd ratios in the inclusions (30 ± 9; 2σ standard deviation) are higher than the canonical ratio observed in oceanic lavas, and Cl/K ratios (0.079 ± 0.028) fall in the range of pristine mantle (0.02–0.08).

1. Introduction

Isotopic measurements performed on ocean island basalts (OIBs) have demonstrated that the Earth's mantle is compositionally heterogeneous [e.g., *Gast et al.*, 1964; *Allègre*, 1982; *Zindler et al.*, 1982; *Zindler and Hart*, 1986; *Hart*, 1988; *Hofmann*, 1997; *White*, 2010]. Although the cause of the chemical heterogeneity in the mantle has been a point of discussion in the scientific community for half a century [*Gast et al.*, 1964], it has been suggested to arise from the subduction of oceanic and continental crust material into the mantle [*Cohen and O'Nions*, 1982; *Hofmann and White*, 1982; *White and Hofmann*, 1982]. Different types of subducted material (e.g., oceanic crust, continental crust, and sediment) have been proposed to give rise to specific mantle end-member isotopic compositions—HIMU (high $\mu = {}^{238}U/{}^{204}Pb$), EM1 (enriched mantle I), and EM2 (enriched mantle II)—which are then melted and erupted as OIB melts at hot spots. EM2 is generally considered to be derived from continental material [*White and Hofmann*, 1982; *Jackson et al.*, 2007], but the origin of EM1 remains more controversial [e.g., *Weaver*, 1991; *Eiler et al.*, 1995; *Eisele et al.*, 2002; *Honda and Woodhead*, 2005; *Salters and Sachi-Kocher*, 2010; *Hart*, 2011]. The HIMU mantle end-member is thought to be derived from ancient subducted oceanic crust [e.g., *Chase*, 1981; *Hofmann and White*, 1982; *Zindler et al.*, 1982; *Nakamura and Tatsumoto*, 1988; *Dupuy et al.*, 1989; *Graham et al.*, 1992; *Hauri and Hart*, 1993; *Hémond et al.*, 1994; *Roy-Barman and Allegre*, 1995; *Woodhead*, 1996; *Hanyu and Kaneoka*, 1997;

Kogiso et al., 1997; *Salters and White*, 1998; *Schiano et al.*, 2001; *Lassiter et al.*, 2003; *Stracke et al.*, 2003; *Stroncik and Haase*, 2004; *Nishio et al.*, 2005; *Chan et al.*, 2009; *Parai et al.*, 2009; *John et al.*, 2010; *Hanyu et al.*, 2011; *Kawabata et al.*, 2011; *Salters et al.*, 2011; *Krienitz et al.*, 2012; *Cabral et al.*, 2013]. Because of the fluid mobility of Pb during subduction zone processing, Pb loss from the slab results in high U/Pb ratios in the subducted slab reservoir, which evolves highly radiogenic Pb-isotope compositions over time [*Hofmann and White*, 1982; *Zindler and Hart*, 1986; *Hauri and Hart*, 1993; *Kelley et al.*, 2005; *Hanyu et al.*, 2011, 2014]. Alternatively, the high U/Pb inferred for the HIMU mantle source may be a result of U incorporation into oceanic crust during submarine alteration [*Hart and Staudigel*, 1982; *Hofmann and White*, 1982; *Chauvel et al.*, 1992; *Kelley et al.*, 2003], and this elevated U/Pb ratio preserved during subduction would evolve the radiogenic Pb-isotopic signature associated with the HIMU mantle domain [*Chase*, 1981; *Hofmann and White*, 1982]. A recycled origin for the HIMU mantle end-member has been further supported by sulfur isotopic measurements from olivine-hosted melt inclusions from Mangaia, which confirm that the material erupted at Mangaia was once at Earth's surface >2.45 billion years ago [*Cabral et al.*, 2013].

During its life on the seafloor, oceanic lithosphere, including crust, experiences low temperature alteration and becomes H_2O-rich and CO_2-rich (and gains up to several weight percent H_2O and CO_2 in the top portion of the crust during submarine alteration) [e.g., *Staudigel et al.*, 1996; *Alt and Teagle*, 1999; *Bach et al.*, 2001; *Wallmann*, 2001; *Dixon et al.*, 2002; *Gillis and Coogan*, 2011]. If the HIMU mantle end-member is truly composed of subducted oceanic crust that is subsequently melted and erupted, this mantle end-member can present important insights into how volatiles are returned to the mantle and recycled back to the surface at hot spots. This is important, as the distribution of volatiles in the mantle (particularly H_2O) is a significant variable in determining the rheology of the mantle, the depth and extent of mantle melting, as well as the composition of melts and how they evolve [e.g., *Hirth and Kohlstedt*, 1996; *Gaetani and Grove*, 1998; *Asimow and Langmuir*, 2003; *Hirschmann*, 2006; *Portnyagin et al.*, 2007]. The results of *Cabral et al.* [2013] also demand that the HIMU mantle sampled by Mangaia lavas experiences long-term storage in the mantle, which has important implications for mantle dynamics and the mechanisms of long-term mantle storage for this end-member. This discovery highlights the need for careful geochemical characterization of HIMU lavas from Mangaia to better understand the origins of this mantle end-member. Despite its importance for understanding mantle recycling processes, from subduction zones to hot spots, volatile measurements are not available from the extreme HIMU mantle end-member sampled by Mangaia lavas.

Due to the lack of deep sea dredging expeditions in the Cook Islands, submarine volcanic glasses are not available for volatile abundance characterization of HIMU mantle end-member lavas from Mangaia. Volatiles have not been measured on HIMU mantle end-member lavas, which extend to $^{206}Pb/^{204}Pb$ values of 21.9 in high-precision measurements made on basalts from Mangaia Island [e.g., *Hauri and Hart*, 1993; *Woodhead*, 1996; *Kogiso et al.*, 1997; *Hanyu et al.*, 2011]. In an effort to obtain volatile measurements of this end-member, we have homogenized crystalline melt inclusions hosted in olivine phenocrysts extracted from subaerially erupted whole rocks collected from Mangaia. These analyses represent the first coupled Pb isotope and major, volatile, and trace element compositions measured on glasses from the HIMU mantle end-member.

We find that Mangaia melt inclusions host H_2O and CO_2 concentrations that are relatively high (1.73 wt % and 2346 ppm, respectively; corrected for olivine fractionation). We use the new data to constrain volatile abundances in the HIMU mantle end-member as well as volatile cycling in the mantle, from subduction zones to hot spots.

2. Sample Descriptions, Locations, and Methods

Sample descriptions and locations, as well as a description of the geology of Mangaia, are provided in the supporting information. A complete description of melt inclusion preparation (including the homogenization procedure) and methods for analysis of Pb-isotopes and major, trace, and volatile concentrations are also provided in the supporting information.

3. Results

The melt inclusions in this study are alkalic (Figure 1). The forsterite values of the olivine hosting the inclusions in this study range from 75.9 to 86.1, with an average of 81.6 (supporting information Table S1). The
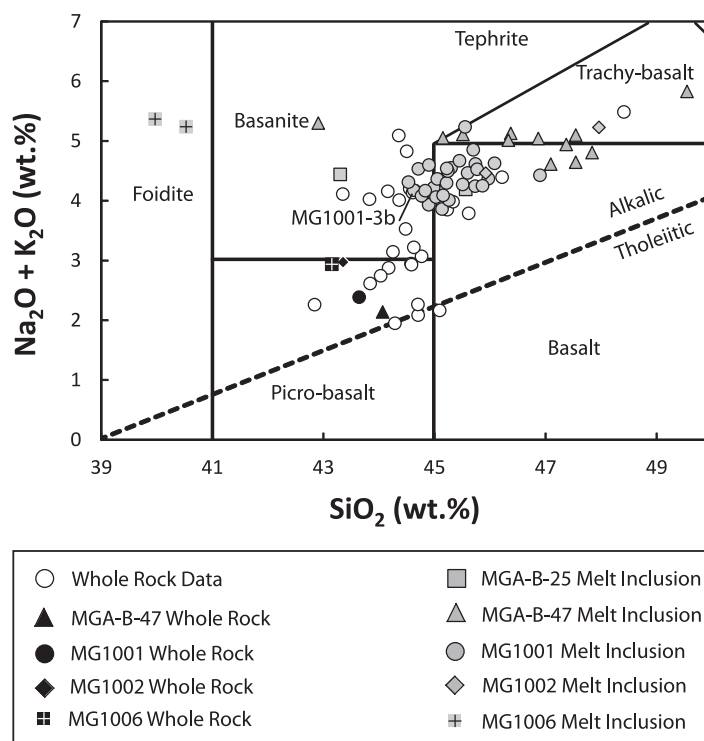
Figure 1. $Na_2O + K_2O$ versus SiO_2 plotted with the alkali-tholeiite basalt line from *MacDonald and Katsura* [1965] and applicable rock types. Mangaia melt inclusions are plotted as gray symbols and were corrected for olivine addition or subtraction (following the methods outlined in *Jackson et al.* [2012]) to be in equilibrium with their host olivine (see supporting information Table S5 for olivine-corrected concentrations). The whole rocks hosting the respective melt inclusions are plotted as the same symbol as the melt inclusions, but in black. Previously published whole rock data are shown as white circles and were obtained from Georoc [*Sarbas*, 2008]. One sample (M17) from *Woodhead* [1996] contains anomalously low Na_2O. We argue that this is a result of significant alteration, which is supported by the high loss on ignition (LOI) of 9.33% for this sample; we have removed this sample from the figures. Whole rock data for MGA-B-25 is not available. Samples from this study plot in the alkalic field.

largest range in forsterite content is exhibited by olivines from hand sample MGA-B-47 (Fo = 80.3–86.1, supporting information Tables S1 and S2). The melt inclusion data presented in Figure 2 have been corrected to be in equilibrium with the host olivine by addition or subtraction of equilibrium olivine following the methods outlined in *Jackson et al.* [2012], and discussion of the major, trace, and volatile element data below refers to abundances following this olivine fractionation correction, unless stated otherwise (supporting information Tables S1 and S3–S5). The MgO contents of the melt inclusions do not span the entire range encapsulated by the whole rocks (3.10–20.47 wt %); instead they are restricted to a range of 4.51–10.80 wt % MgO (supporting information Table S5). The melt inclusions tend to have lower MgO than the host whole rocks, and this likely owes to the fact that the whole rocks examined in this study are phenocryst-rich and therefore may reflect cumulate composi-

tions. The SiO_2 concentrations generally cluster in the range defined by whole rocks from Mangaia, but some inclusions (mostly from MGA-B-47) exhibit somewhat higher SiO_2 at a given MgO than the whole rocks. Two inclusions in particular (both from hand sample MG1006) have lower SiO_2 than previously identified in Mangaia lavas. The whole rock data suggest the crystallization of a Ti-rich phase in lavas where MgO reaches <5 wt %. The melt inclusion MgO concentrations are generally above 5 wt % (with the exception of sample MGA-B-47-RAC3 with 4.51 wt % MgO, corrected for olivine fractionation) and, with the possible exception of MGA-B-47-RAC3, do not reach the point of extreme magmatic evolution where TiO_2 concentrations are affected by fractionation of the Ti-rich phase. In sample MGA-B-47, there is one inclusion with TiO_2 significantly higher than the whole rock and melt inclusion analyses. The melt inclusions generally overlap with whole rock data in a plot of Al_2O_3 versus MgO (Figure 2). At a given MgO, most of the inclusions plot within the range of whole rocks for K_2O and Na_2O, but a large subset of the inclusions is shifted to higher alkali element concentrations than observed in the whole rocks. Melt inclusions generally have CaO concentrations and CaO/Al_2O_3 ratios that are similar to the whole rock data at a given MgO, except for inclusions from sample MGA-B-47, which have higher CaO, and a single inclusion from MG1001, which has lower CaO. There is a clear depletion in FeO for melt inclusions from the MGA-B-47 whole rock, which has been observed in melt inclusions previously and predicted experimentally (discussed below) [*Danyushevsky et al.*, 2000; *Gaetani and Watson*, 2000]. Melt inclusions from the other samples lie on the FeO versus MgO trend formed by whole rocks, except for the two melt inclusions from the MG1006 whole rock, which show an elevation in FeO compared to the rest of the melt inclusion and whole rock data. These two inclusions are anomalous in many respects, and have the lowest SiO_2, among the lowest CaO and CaO/Al_2O_3, and among the highest alkali abundances in the melt inclusion suite.

Figure 2. Major element variability in Mangaia melt inclusions compared to their respective whole rocks and previously published whole rocks from the island. Samples from this study use the same symbol convention as seen in Figure 1. Error bars in the corner of each plot represent the average 2σ measurement error of the melt inclusions. Data shown are for melt inclusions that have been corrected to be in equilibrium with the host olivine (see supporting information Table S5 for olivine-corrected concentrations).

Previously published whole rock trace element data were obtained from the Georoc database [*Sarbas*, 2008] and, with few exceptions (see caption of Figure 3), were filtered for trace element analyses made by ICP-MS (inductively coupled plasma mass spectrometry) [*Hauri and Hart*, 1993; *Woodhead*, 1996; *Hanyu*

Figure 3. Trace element spidergrams of Mangaia melt inclusions compared to Mangaia whole rocks. Mangaia melt inclusion data (corrected for olivine fractionation to be in equilibrium with the host olivine, see supporting information Table S5) are plotted as black lines, except for inclusion MG1001-5, which is plotted as a gray dashed line. All data are normalized to the chondrite-based primitive mantle values of *McDonough and Sun* [1995]. (a) Previously published whole rock trace element data were acquired from Georoc [*Ha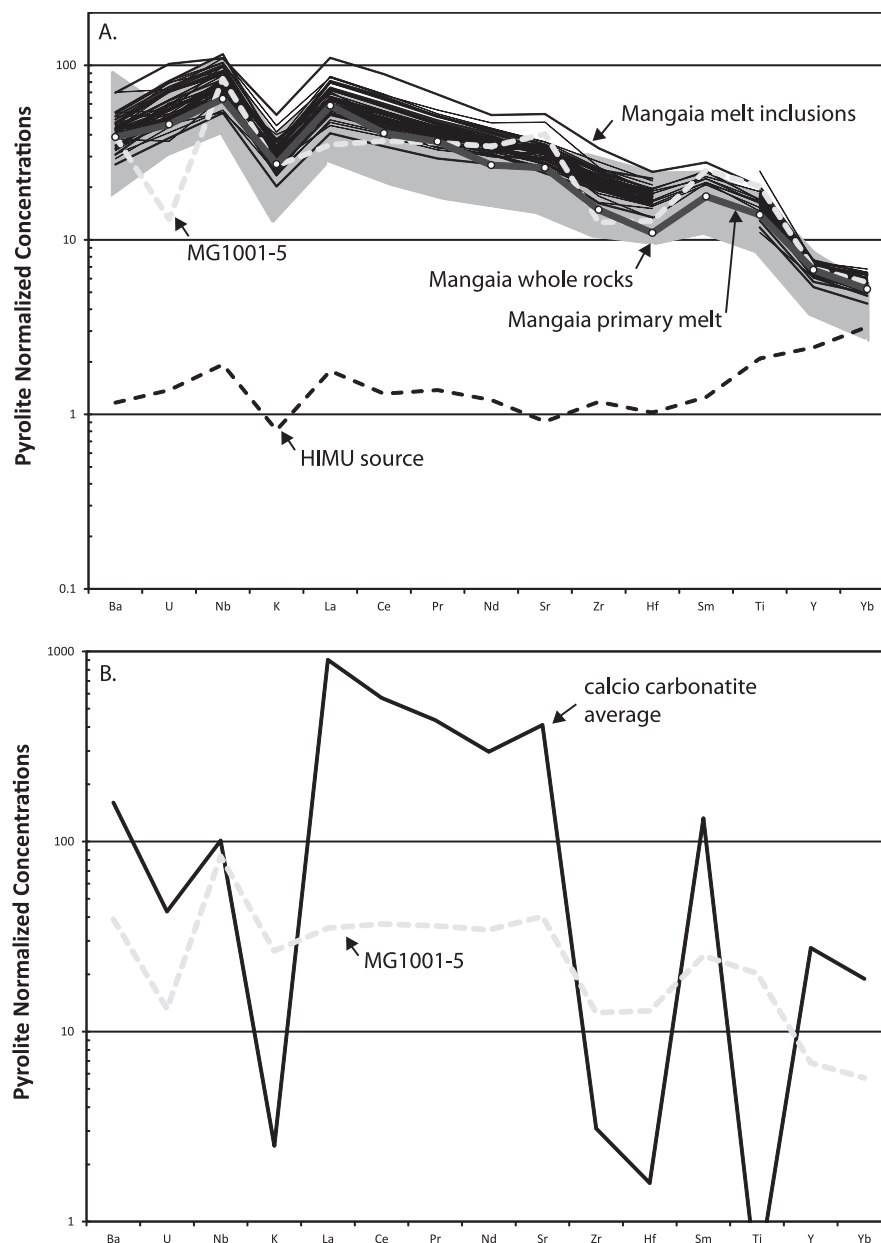uri and Hart*, 1993; *Woodhead*, 1996; *Sarbas*, 2008; *Hanyu et al.*, 2011] and were filtered to include only samples with a full suite of trace element data (Ba, U, Nb, La, Ce, Pr, Nd, Sr, Zr, Hf, Sm, Y, and Yb) obtained by ICP-MS analysis (except for Zr from *Hauri and Hart* [1997], which was measured by XRF). A complete set of trace element data by ICP-MS did not exist from *Kogiso et al.* [1997], so we exclude the data from this reference from the figure. Only whole rock samples that have MgO compositions >5 wt % are plotted to avoid the effects of extreme crystal fractionation (the majority of melt inclusions in this study have more than 5 wt % MgO). Additionally, whole rock samples with greater than 4% LOI are also excluded from the figure to avoid effects of alteration. The estimated primary melt concentration for Mangaia, calculated from inclusion MG1001-3b following olivine fractionation corrected to be in equilibrium with mantle olivine (with forsterite 90 composition), is the following (in ppm): Ba = 256.0, U = 0.93, Nb = 42.3, K = 6511, La = 38.0, Ce = 68.4, Pr = 9.3, Nd = 33.5, Sr = 515, Zr = 156, Hf = 3.1, Sm = 7.2, Ti = 16,750, Y = 28.9, Yb = 2.3. Using the melt model outlined in section 3.2, ~3% melting of the HIMU mantle source (shown as a black dashed line) will generate this primary melt composition if the trace element concentrations in the source are the following (in ppm): Ba = 7.7, U = 0.028, Nb = 1.27, K = 195, La = 1.15, Ce = 2.20, Pr = 0.35, Nd = 1.51, Sr = 18.1, Zr = 12.4, Hf = 0.29, Sm = 0.51, Ti = 2520, Y = 10.4, Yb = 1.4. (b) Melt inclusion MG1001-5—which has an anomalous spidergram pattern—plotted as a gray dashed line. It is compared to the average of Cape Verde calcio-carbonatites from Fuerteventura Island [*Hoernle et al.*, 2002], which is plotted as a solid black line. Inclusion MG1001-5 has several geochemical similarities with thee calico-carbonatite average, including negative anomalies of U, K, Zr, Hf, and positive anomalies of Nb and Sr. However, the inclusion does not have the negative Ti anomaly found in the carbonatite.

et al., 2011]. The whole rock trace element data and the new melt inclusion trace element data are shown as spidergrams in Figure 3. The majority of the melt inclusion trace element data agree well with the previously published whole rock trace element data. One exception is inclusion MG1001-5 (dashed gray line in Figure 3), which has a spidergram pattern significantly different than the other melt inclusions and previously published whole rocks. This sample was subjected to two replicate analyses by SIMS at Arizona State University, and an additional analysis by LA-ICP-MS at URI (supporting information Table S3), and the replicate analyses gave the same spidergram pattern. A key feature of this melt inclusion is that the spidergram has strongly negative Zr and Hf anomalies, which mimic more subtle negative Zr and Hf anomalies in HIMU lavas from Mangaia [*Kogiso et al.*, 1997; *Hanyu et al.*, 2011] and other OIBs from the Cook-Austral Islands [*Chauvel et al.*, 1997]. Notably, this inclusion does not have anomalous major or volatile element abundances. The trace element pattern is qualitatively similar to the average calcio-carbonatite (including trace phases, like apatite, that are associated with calcio-carbonatite) from Fuerteventura (Cape Verde hot spot) presented by *Hoernle et al.* [2002], including negative anomalies U, K, Zr, Hf, and positive anomalies of Nb and Sr. However, the inclusion does not have the negative Ti anomaly found in the calcio-carbonatites, and we cannot offer an explanation for the origin of the anomalous trace element pattern in this inclusion.

The Mangaia melt inclusions are characterized by high H_2O and CO_2 contents (Figure 4a), up to 1.73 wt % and 2346 ppm (supporting information Table S5 and Figure 4b). Inclusions from MGA-B-47 form a separate group with lower H_2O than the melt inclusions from other hand samples; melt inclusions from this sample also appear to have lower abundances of FeO (Figure 2) and H_2O. The lower H_2O (and H_2O/Ce, see below) in inclusions from this sample suggest water loss from the inclusion through the host olivine (see section 4.1). An inclusion from sample MG1006 exhibits high CO_2, but like MGA-B-47 it has low H_2O abundances (1750 ppm and 0.57 wt %, respectively; supporting information Table S5). However, unlike MGA-B-47 inclusions, this inclusion does not exhibit evidence for lower FeO abundance. Excluding this inclusion and all inclusions from MGA-B-47, the majority of the Mangaia melt inclusions lie along a broad array centered at ~1.5 wt % H_2O (varying from 1.14 to 1.73 wt %, supporting information Table S5). This array, defined by 27 inclusions from hand sample MG1001 and three inclusions from hand sample MGA-B-25 only, spans CO_2 concentrations ranging from 284 to 2346 ppm (supporting information Table S5). Excluding melt inclusion samples from MGA-B-47 (discussed below), the melt inclusions record entrapment pressures ranging from 250 bar to approximately 1.75 kbar (see Figure 4a). This translates to entrapment depths of up to 6.4 km (1.75 kbar) for melt inclusions with the highest concentrations of CO_2 (assuming a rock density of igneous crust of 2800 kg/m^3) [*Workman et al.*, 2006].

Figure 4c provides ratios of volatile (H_2O and CO_2) to nonvolatile (Ce and Nb) trace elements that have similar mineral-melt partition coefficients during mantle melting and magmatic differentiation processes. Excluding MGA-B-47 and MG1006 inclusions, H_2O/Ce varies from 119 to 245; the highest H_2O/Ce value (245; sample MG1001A12) is associated with the highest (least degassed) CO_2/Nb ratio (49.5; sample MG1001A12), but this inclusion exhibits evidence for assimilation (see below).

Koleszar et al. [2009] suggested that the MORB mantle has a CO_2/Nb ratio of 300 [*Koleszar et al.*, 2009], but CO_2/Nb in the various mantle reservoirs may not be constant, and it has also been suggested that the OIB mantle may have higher CO_2/Nb than the MORB mantle [*Saal et al.*, 2002; *Cartigny et al.*, 2008; *Koleszar et al.*, 2009]. The Mangaia melt inclusions reach a maximum CO_2/Nb value of only 49.5, suggesting significant degassing (see section 4.4), and CO_2 and CO_2/Nb ratios in the inclusions must still be viewed as minimum values.

Fluorine concentrations range from 1073 to 1950 ppm (supporting information Table S5) in the Mangaia melt inclusions. When compared to Nd, they are offset to higher F/Nd (~30) than the F/Nd ratio of 21 observed in other MORB and OIB samples (Figure 5) [e.g., *Workman et al.*, 2006]. F/Nd may not always reflect mantle source characteristics if assimilation and alteration processes are involved. For example, *Lassiter et al.* [2002] studied a HIMU lava from Raivavae (sample RVV318, $^{206}Pb/^{204}Pb = 20.94$) that showed strong evidence for brine and oceanic crust assimilation—and melt inclusions from this sample have high F/Nd ratios (60–183). *Koleszar et al.* [2009] also identified high F/Nd in five melt inclusions that range from approximately 35 to 100 and argue that this departure from the canonical ratio of fresh OIBs and MORBs of 21 may relate to open-system behavior of F. We note that the Mangaia melt inclusion suite has elevated F/Nd ratios, but these inclusions do not exhibit signatures associated with significant assimilation prior to entrapment (see discussion, Figure 6).

Cl/K_2O ratios for the Mangaia melt inclusions are quite low (Figure 6). The average Cl/K_2O of the melt inclusions is 0.067 (including melt inclusions from MGA-B-47), which corresponds to a Cl/K ratio of 0.079 ± 0.028 and overlaps with the range for pristine oceanic lavas ($Cl/K = 0.02–0.08$) found by *Michael and Cornell* [1998] and *Stroncik and Haase* [2004].

Figure 7 compares Cl/Nb and F/Nd ratios in the Mangaia inclusions. Cl/Nb ratios, like Cl/K ratios, can be used to monitor for assimilation of altered oceanic crust or brines (see discussion section 3.5). While the $F/$
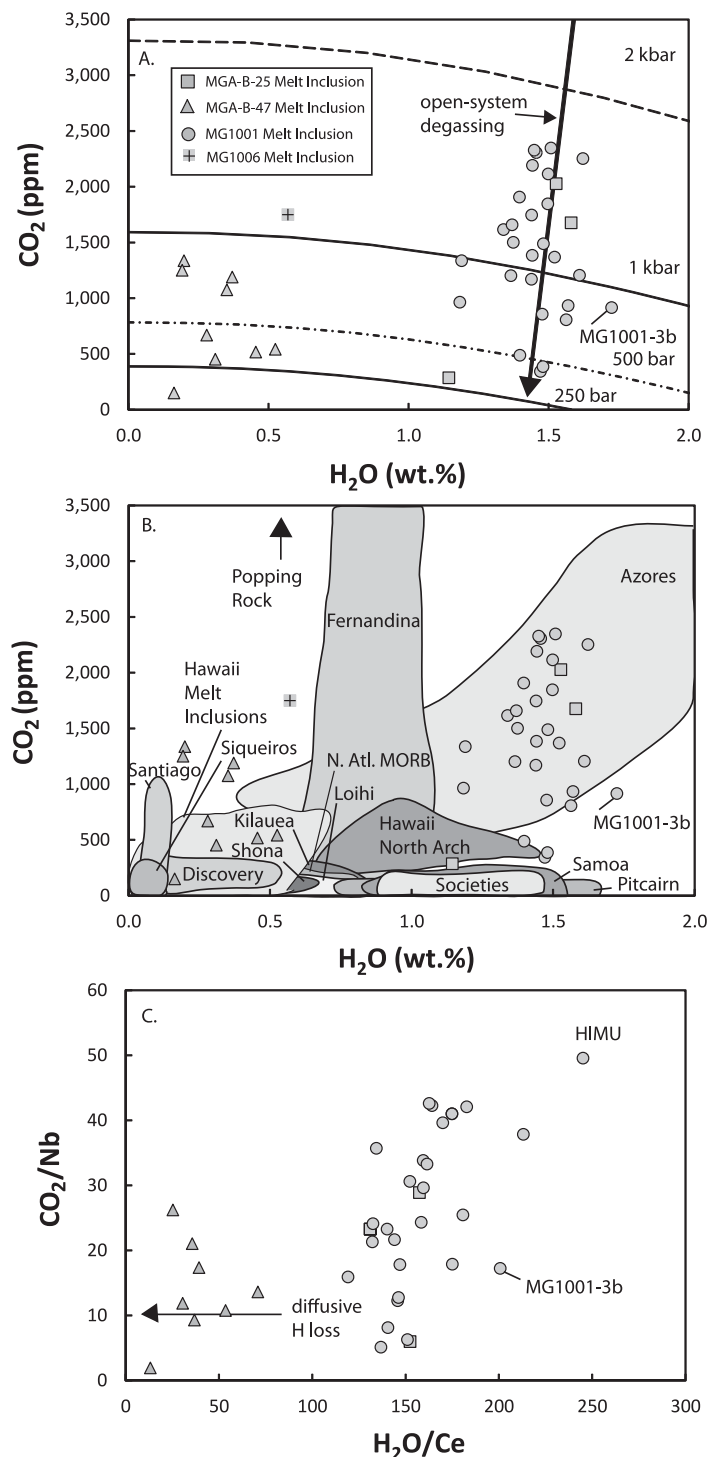

Figure 4.

Nd in the Mangaia inclusions is shifted to higher values than observed in the EM1 and EM2 hot spots (Pitcairn, Samoa, and Societies), even higher F/Nd ratios are found in melts from the Azores, Galapagos, and Australs hot spots.

Sulfides are abundant in Mangaia melt inclusions. Data for S concentrations in the silicate portions of the melt inclusions are provided in supporting information Table S4. Since the concentration of S in the silicate portion of the inclusions is buffered by the presence of sulfides, we cannot use the measured S concentrations to make inferences about sulfur in the mantle source and we do not discuss sulfur further in this paper. Some measurements of Pb isotopes, S isotopes, and major elements of the sulfides from these inclusions can be found in *Cabral et al*. [2013]. Sulfides from samples MGA-B-25 and MGA-B-47 were found to have anomalous sulfur isotopic compositions that indicate mass independent fractionation [*Cabral et al.*, 2013].

Excluding melt inclusion measurements where the ion probe primary beam overlapped with phase boundaries (see supporting information), new measurements (supporting information Table S5) of Pb-isotopic ratios in the Mangaia inclusions plot in a tighter cluster near the extreme HIMU mantle end-member defined by Mangaia whole-rock compositions (Figure 8). The limited isotopic variability of the new SIMS measurements presented here for homogenized and nonhomogenized melt inclusions is similar to that observed in the *Paul et al*. [2011] LA-ICP-MS study. We do not observe the significant variability in Pb-isotopic measurements in melt inclusions identified in previous SIMS studies of Mangaia inclusions [*Saal et al*., 1998, 2005; *Yurimoto et al*., 2004]. Melt inclusions from MGA-B-25 ($n = 4$ different inclusions analyzed) show the least Pb-isotopic variability, while MGA-B-47 exhibits the most Pb-isotopic variability ($n = 12$ different inclusions analyzed). MG1001 exhibits intermediate isotopic variability ($n = 23$ inclusions analyzed). Only one melt inclusion was analyzed from sample MG1002, and no melt inclusions from MG1006 were analyzed. The sample with the greatest range in olivine forsterite contents, MGA-B-47, also has the most heterogeneous Pb-isotopic compositions.

The new Pb-isotopic data in these melt inclusions exhibit approximately twice as much variability as observed in high-precision Pb-isotopic measurements of leached whole rocks from the island. One melt inclusion plots away from the other melt inclusions in Pb-isotopic space (MGA-B-47-RAC3), and expands the melt inclusion data field significantly; without this single inclusion, the melt inclusion data field is only slightly larger (but shifted to somewhat higher $^{207}Pb/^{206}Pb$ and $^{208}Pb/^{206}Pb$ ratios) than the data field defined by high-precision Pb-isotopic measurements of leached whole rocks from Mangaia.

4. Discussion

In order to constrain volatile element abundances of primary magmas and to ultimately make inferences about the composition of the HIMU mantle sampled by Mangaia lavas, it is first necessary to identify processes that operate on magmas during ascent and eruption that might modify the volatile budgets of the magmas. In the case of melt inclusions, such processes can include degassing before entrapment of the melt inclusion, diffusive H_2O loss from the melt inclusion through the host olivine, and assimilation of

Figure 4. Volatile contents of Mangaia melt inclusions. All Mangaia melt inclusions plotted in this figure are corrected to be in equilibrium with the host olivine (see supporting information Table S5). (a) CO_2 and H_2O contents of the Mangaia melt inclusions with vapor saturation curves generated by SolEx [*Witham et al.*, 2012] and the open-system degassing trend for alkali basalt from *Dixon et al.* [1997]. Major element data from one of the most primitive and undegassed samples in the suite (MG1001-5, corrected for olivine fractionation) was used for the input values to SolEx. Melt inclusions from MGA-B-47 have experienced diffusive water loss and water data for these inclusions are not included in subsequent figures; an inclusion from MG1006 has similarly low water, which is excluded in subsequent figures. As in *Workman et al.* [2006], we interpret the nearly vertical trend (marked by steeply sloping arrow in the top plot) defined by inclusions from sample MG1001 ($n = 27$ inclusions) and MGA-B-25 ($n = 3$ inclusions) to indicate CO_2 degassing with negligible water loss prior to melt inclusion entrapment (except for inclusions from MGA-B-47, which suffered diffusive H-loss post entrapment). (b) The Mangaia melt inclusion data in comparison to other OIB and MORB data sets, which consist of data obtained from submarine glasses and melt inclusions. Data for the high CO_2 inclusions from the Galapagos (Fernandina and Santiago; *Koleszar et al.*, 2009) are ones for which CO_2 from the vapor bubble was calculated back into the melt composition, and this may explain the unusually high CO_2 (extends up to 5821 ppm) in some of the Fernandina inclusions (A. Saal, personal communication, 2014); when a similar calculation is applied to Mangaia melt inclusions, the concentration of CO_2 increases by $< 4\%$ on average and $< 0.02\%$ for H_2O on average (see corrected CO_2 and H_2O values in supporting information Table S4). Additionally, in this figure, samples were removed from plotting if the relevant data source [*Clague et al.*, 1995; *Dixon et al.*, 1997; *Dixon and Clague*, 2001; *Dixon et al.*, 2002; *Hauri*, 2002; *Saal et al.*, 2002; *Workman et al.*, 2006; *Cartigny et al.*, 2008, and references therein; *Koleszar et al.*, 2009; *Kendrick et al.*, 2014; *Metrich et al.*, 2014] indicated that the sample was severely degassed due to shallow eruption, experienced extensive assimilation, or was otherwise compromised; all samples removed, and the reason for their removal, are outlined in the supporting information. (c) CO_2/Nb and H_2O/Ce ratios for Mangaia melt inclusions.
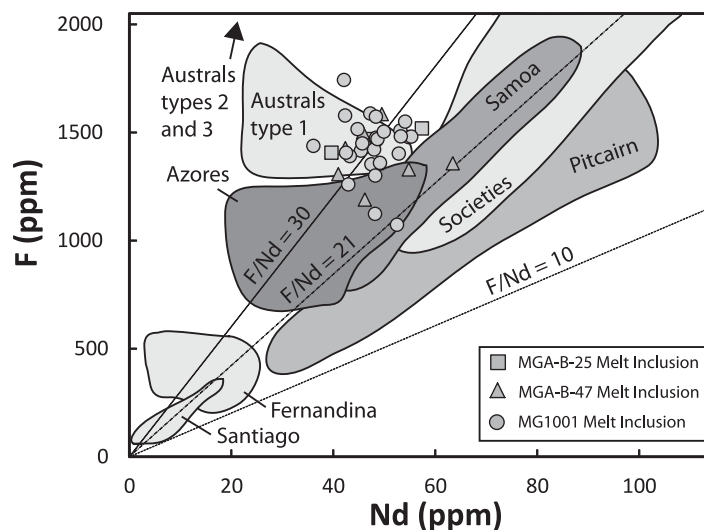
Figure 5. Fluorine versus neodymium of Mangaia melt inclusions in comparison to other OIBs and MORBs. Mangaia melt inclusions are corrected to be in equilibrium with their host olivine (supporting information Table S5) and are shown as gray symbols following the format of previous figures. Other OIB and MORB data are shown for comparison and consist of data obtained from submarine glasses and melt inclusions [*Lassiter et al.*, 2002; *Workman et al.*, 2006; *Koleszar et al.*, 2009; *Kendrick et al.*, 2014; *Metrich et al.*, 2014]. Data were filtered for degassing and assimilation as in Figure 4, with the exception of the data from the Australs: Austral samples are divided into three categories, following *Lassiter et al.* [2002]: Type 1 inclusions are not thought to have experienced assimilation, Type 2 inclusions (which plot outside the figure) are thought to indicate the assimilation of Cl-rich brines, and Type 3 inclusions (which also plot outside the figure) are thought to be secondary inclusions. Mangaia melt inclusions cluster around an average value of F/Nd of approximately 30, which is higher than the "canonical" F/Nd ratio for OIB and MORB of 21 [e.g., *Workman et al.*, 2006]. MGA-B-47 data are shown because, unlike H, F does not show evidence of loss from the inclusion.

altered oceanic crust and brines before entrapment. When evaluating the geochemistry of olivine-hosted melt inclusions from Mangaia, it is critical to evaluate all of these processes to determine whether primary magmatic characteristics can be inferred from this new suite of melt inclusions. Identification of primary melt volatile characteristics permits inferences about the mantle source composition of the HIMU end-member and, thus, volatile cycling through the mantle resulting from subduction-injection of oceanic crust.

4.1. Volatile Element Concentrations: Source Versus Process
4.1.1. Diffusive Loss of Fe and H

Melt inclusions from whole rock sample MGA-B-47 show marked depletion in FeO compared to melt inclusions from the other three whole rock samples, which we interpret to be representative of Fe loss from the inclusions via diffusion through the host olivine (Figure 2). Fe loss from olivine-hosted melt inclusions has been documented in other melt inclusion suites and is thought to occur following long-term storage and slow cooling in the host magma, where the residence time is sufficient to permit Fe diffusion through the olivine [e.g., *Danyushevsky et al.*, 1992, 2000; *Sobolev and Danyushevsky*, 1994; *Gaetani and Watson*, 2000]. The diffusivity of H in olivine is greater than Fe, and if sufficient time elapsed for significant Fe loss to occur, then the time scale for diffusive H-loss from the inclusions was also surpassed and H loss would have taken place provided the external melt had lower H_2O than the melt inclusions. The lower H_2O in MGA-B-47 inclusions is not likely due to magma degassing, as inclusions from MGA-B-47 have elevated CO_2 (149–1335 ppm, supporting information Table S5), so the inclusions were trapped at great depths before significant degassing of H_2O. Therefore, we interpret the low H_2O concentrations in MGA-B-47 inclusions (0.16–0.70 wt %, supporting information Table S5) to be a result of diffusive water loss from the inclusions from this hand sample, and the paired Fe loss and H_2O loss in inclusions are complementary and indicative of longer time scales of storage in a magma chamber following olivine entrapment of the inclusions. Thus, in the discussion below regarding water abundances in the HIMU mantle, we exclude the inclusions from hand sample MGA-B-47.

Melt inclusions from the other hand samples exhibit no evidence for Fe loss, and have FeO abundances similar to previously published whole rocks from Mangaia. The other inclusions also have H_2O (and H_2O/Ce) concentrations that are higher than the H_2O in MGA-B-47. Diffusive loss from the inclusions via the olivine, or diffusive incorporation of water into the melt inclusion, is unlikely to have occurred in inclusions from MGA-B-25 and MG1001. The inclusions from these two lavas form overlapping arrays in plots of CO_2 versus H_2O and CO_2/Nb versus H_2O/Ce (Figure 4). It would seem unlikely that diffusive water loss or incorporation in inclusions from two different lavas would generate the same arrays by coincidence, though we note that the arrays are biased by a single inclusion with the highest CO_2/Nb versus H_2O/Ce. Diffusive loss of H from the inclusions may occur following eruption during slow cooling of lavas, but it is difficult to rule out such a mechanism
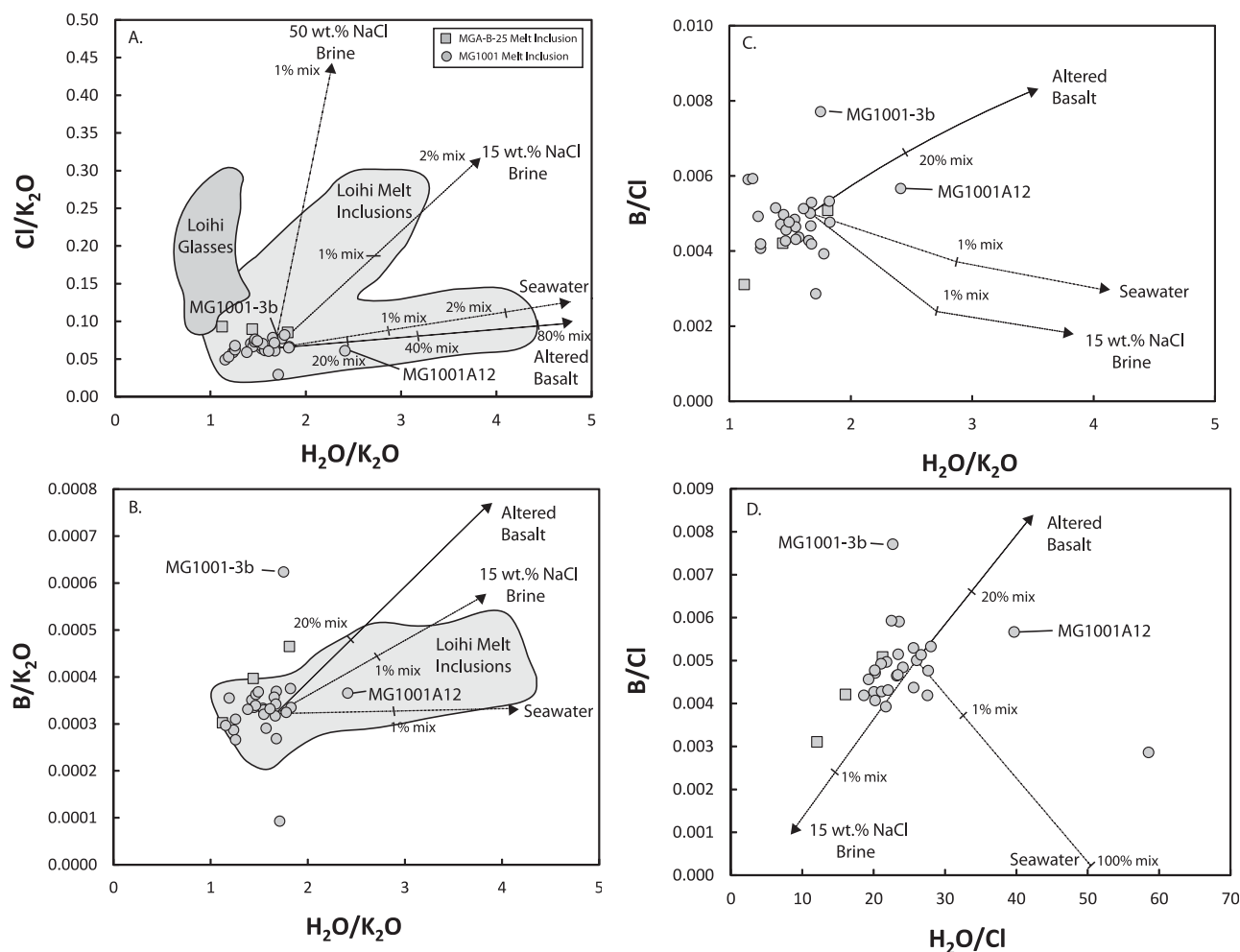
Figure 6. Mixing models demonstrating the effect of assimilating different crustal and brine materials. Mangaia melt inclusion data are plotted as gray symbols following previous figure formatting. Loihi melt inclusion data are outlined in a light gray field and a dark gray field outlines Loihi pillow glasses [*Kent et al.*, 1999a, and references therein]. The model lines and end-member compositions (altered basalt, seawater, and two different brine compositions) for the assimilation model are from *Kent et al.* [1999a]. The Mangaia primary magma in the model uses olivine fractionation corrected data from melt inclusion MG1001-14 to define the primary basalt composition because it has the most primitive MgO content (10.8 wt %, corrected for olivine fractionation, see supporting information Table S5) in the inclusion suite. Like most of the inclusions in this study, MG1001-14 has a relatively low Cl/K_2O ratio (0.064) typical of mantle-derived lavas that have not experienced significant assimilation of hydrothermally altered material. Notably, the composition of one melt inclusion (MG1001A12, which also has the highest H_2O/K_2O and H_2O/Ce in the melt inclusion suite) may be explained by the assimilation of altered basalt and/or seawater, and this sample is indicated in all plots of this figure. Data from MGA-B-47 and MG1006 inclusions are not shown owing to diffusive water loss.

lowering the H_2O in the melt inclusions from the primary magmatic values. For example, there is no clear relationship between H_2O and Ce in the inclusions. However, owing to the fact that small melt inclusions are more susceptible to diffusive loss of H_2O than larger inclusions [*Chen et al.*, 2011], a positive relationship between H_2O and melt inclusion diameter will be present if diffusive loss of H_2O has occurred. We observe no such relationship in inclusions from MGA-B-25 and MG1001 (Figure 9), which argues against diffusive loss of H_2O from the inclusions; however, the inclusions from sample MGA-B-47 that have suffered Fe loss and H_2O loss do show a weak relationship between melt H_2O and melt inclusion diameter, which is consistent with diffusive loss of H from inclusions in this sample. However, while diffusive loss from MGA-B-25 and MG1001 inclusions seems unlikely (given the lack of relationship between H_2O and inclusion size), it cannot be ruled out, and the H_2O/Ce ratios in the melt inclusions should be treated as minima. For inclusions from samples MGA-B-25 and MG1001, we also conclude that diffusive exchange through the olivine did not modify the abundance of the other incompatible trace elements, like F, Cl, and S, because their diffusivities are expected to be significantly slower than those of Fe and H [*Cherniak*, 2010; *Bucholz et al.*, 2013].

After excluding inclusions from MGA-B-47, H_2O/Ce ratios exhibit some variability in Mangaia inclusions. While H_2O concentrations and H_2O/Ce ratios are relatively high in the Mangaia melt inclusions (excluding
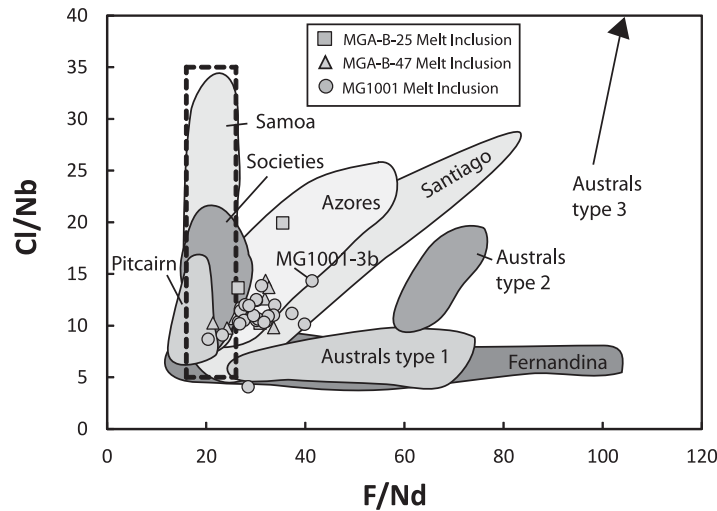
Figure 7. Cl/Nb versus F/Nd for Mangaia melt inclusions compared to global OIBs and MORBs. Mangaia melt inclusion data are plotted as gray symbols following previous figure formatting. The dashed box represents the canonical F/Nd value from *Workman et al.* [2006] and the range of Cl/Nb suggested for the mantle [*Lassiter et al.*, 2002; *Saal et al.*, 2002; *Workman et al.*, 2006; *Koleszar et al.*, 2009; *Shaw et al.*, 2010; *Kendrick et al.*, 2014; *Metrich et al.*, 2014, www.earthchem.org/petdb]. Data from other locations are provided for comparison and consist of data collected from submarine glasses and melt inclusions [*Lassiter et al.*, 2002; *Workman et al.*, 2006; *Koleszar et al.*, 2009; *Kendrick et al.*, 2014; *Metrich et al.*, 2014]. See the caption of Figure 5 for description of Austral sample groups. Data are filtered in the same way as in the caption of Figure 4.
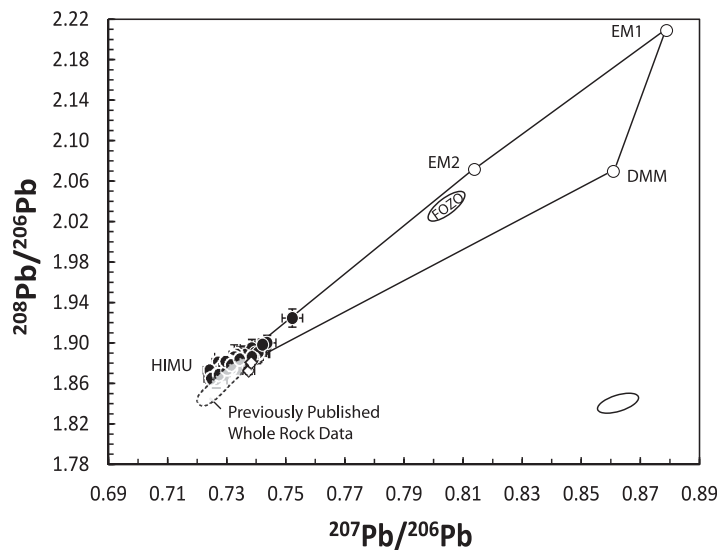

Figure 8. $^{208}Pb/^{206}Pb$ versus $^{207}Pb/^{206}Pb$ measurements on Mangaia melt inclusions from this study. Data from this study obtained on homogenized inclusions are shown as solid black circles (supporting information Table S5). Data from sulfide inclusions are plotted as white diamonds; the average of two analyses is plotted for one of the sulfide analyses (supporting information Table S5). FOZO values are estimated and are from *Hart et al.* [1992]. The field for previously published whole rock basalt data from Mangaia shows only the data obtained from leached whole rocks that were measured by MC-ICP-MS [*Hanyu et al.*, 2011] or by a double-spike TIMS method [*Woodhead*, 1996]. The error ellipse (in the bottom right portion of the figure) represents the 2σ reproducibility (but not the absolute value) of the secondary standard measurements during the session (these measurements are shown individually in supporting information Figure S2).

inclusions from sample MGA-B-47), some H_2O loss may occur by diffusive H_2O loss from inclusions [e.g., *Chen et al.*, 2011; *Gaetani et al.*, 2012] and slight loss of H_2O can occur via degassing prior to inclusion entrapment (see below), and this may explain the lower H_2O/Ce ratios (down to 119) observed in some of the Mangaia inclusions.

4.1.2. Degassing of H_2O and CO_2

Models examining solubility of H_2O and CO_2 in mantle melts have shown that, during open-system degassing, the vapor phase is dominated by CO_2 until very low pressures (~100 bars) [*Dixon*, 1997]. As in *Dixon* [1997] and *Workman et al.* [2006], we interpret the nearly vertical degassing trend (Figure 4a) and entrapment pressures >100 bar to indicate negligible H_2O loss from the melt inclusions from hand samples MG1001 and MGA-B-25.

Owing to the low solubility of CO_2 in mantle melts, in only rare cases has CO_2 been observed to be undersaturated, thereby providing information about primary melt CO_2 abundances [*Saal et al.*, 2002]. In the case of Mangaia, and all other OIB and MORB locations examined to date, extensive degassing of CO_2 is evident. Therefore, primary melt CO_2 abundances cannot be calculated with the present data set, as estimates determined for the primary melt CO_2 concentration using CO_2/Nb ratios have large uncertainties owing to variability in the CO_2/Nb ratio [*Saal et al.*, 2002; *Cartigny et al.*, 2008; see section 4.4], particularly if carbonatite is present during melting [*Dasgupta et al.*, 2009].
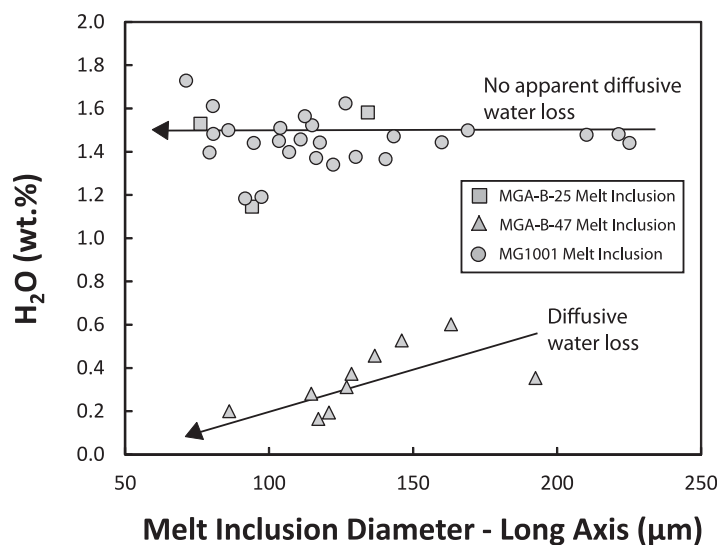
Figure 9. Melt inclusion H_2O contents compared to melt inclusion long axis diameter. Mangaia melt inclusion data are plotted as gray symbols following previous figure formatting. The data have been corrected to be in equilibrium with the host olivine. The lack of correlation for melt inclusions from samples MGA-B-25 and MG1001 suggest no significant diffusive H_2O loss from the inclusion. However, the negative correlation observed for melt inclusions from hand sample MGA-B-47 does suggest diffusive H_2O loss, and is consistent with the previous observations from this study.

Assimilation during magma ascent: Assimilation of oceanic crust and/or brines during ascent and eruption of magma can modify the Cl and H_2O abundances of the magma [*Michael and Schilling*, 1989; *Jambon et al.*, 1995; *Michael and Cornell*, 1998; *Kent et al.*, 1999a, 1999b; *Lassiter et al.*, 2002; *Stroncik and Haase*, 2004; *Kendrick et al.*, 2013a]. *Kent et al.* [1999a] explored this issue through the analysis of matrix glass and olivine-hosted glass inclusions from Loihi sea-mount, Hawaii. Following *Kent et al.* [1999a], we examined the variability of Cl/K_2O and H_2O/K_2O in the melt inclusions from Mangaia (Figure 6). The majority of melt inclusions plot in a small cloud near the most primitive (highest MgO) Man-

gaia melt inclusion composition (see Figure 6 caption for description) and generally exhibit limited variability, especially in comparison with the variability seen in the Loihi samples, which are known to have experienced assimilation. However, we note that assimilation of altered basalt, as shown in Figure 6, can increase the H_2O/K_2O (and H_2O/Ce) without significantly increasing the Cl/K_2O, and thus Cl/K_2O alone cannot be used to evaluate assimilation of altered oceanic basalt. However, in plots showing B/K_2O, H_2O/K_2O, B/Cl, and H_2O/Cl, one inclusion (MG100A12) is systematically shifted in a direction that suggests assimilation of altered oceanic crust and seawater (Figure 6). This inclusion also has the highest H_2O/Ce (245) in the suite, and the high value may owe to assimilation of H_2O. However, the other inclusions do not appear to be shifted consistently in the direction of assimilation of crustal materials, brines, or seawater. These inclusions, which exhibit no clear evidence for assimilation, have H_2O/Ce values that range up to ∼200. However, we cannot exclude the possibility that minor assimilation has occurred in other inclusions in the Mangaia suite, which may result in the incorporation of non-magmatic H_2O. If this is the case, then the H_2O/Ce of the Mangaia HIMU melts will be overestimated. Further work analyzing HIMU samples at other localities, particularly quenched submarine glasses, will be important for constraining the H_2O content of this mantle end-member.

4.2. H_2O in the HIMU Source and Constraints on Cycling of Subducted Oceanic Crust

The crustal recycling origin hypothesis for the HIMU mantle end-member requires that material (oceanic crust) once at the Earth's surface was processed through a subduction zone, experienced long-term storage in the mantle, and was reerupted at an OIB locality, such as Mangaia. The input of water-rich altered oceanic crust to subduction zones may represent a significant contribution of H_2O to the mantle [e.g., *Hacker*, 2008], and data from the Mangaia melt inclusions can provide constraints on the water that remains in the oceanic crust during subduction.

In order to calculate representative H_2O abundances for the HIMU mantle source, it is important to consider the melting process itself. Owing to the incompatibility of H_2O, mantle melting concentrates water in the melt relative to the mantle source and subsequent fractional crystallization further increases the concentration of H_2O in the melt. Comparing H_2O concentrations to the concentrations of other similarly incompatible elements (e.g., Ce and K) provides a means to "see" through the melting process, as H_2O/Ce ratios are not significantly modified during mantle melting to generate OIB and MORB [e.g., *Michael*, 1995; *Dixon et al.*, 2002].

When H_2O is plotted against K_2O and Ce, lavas that erupt at different hot spot localities fall on different trends (Figure 10). Melt inclusions from Mangaia have relatively high H_2O concentrations compared to other
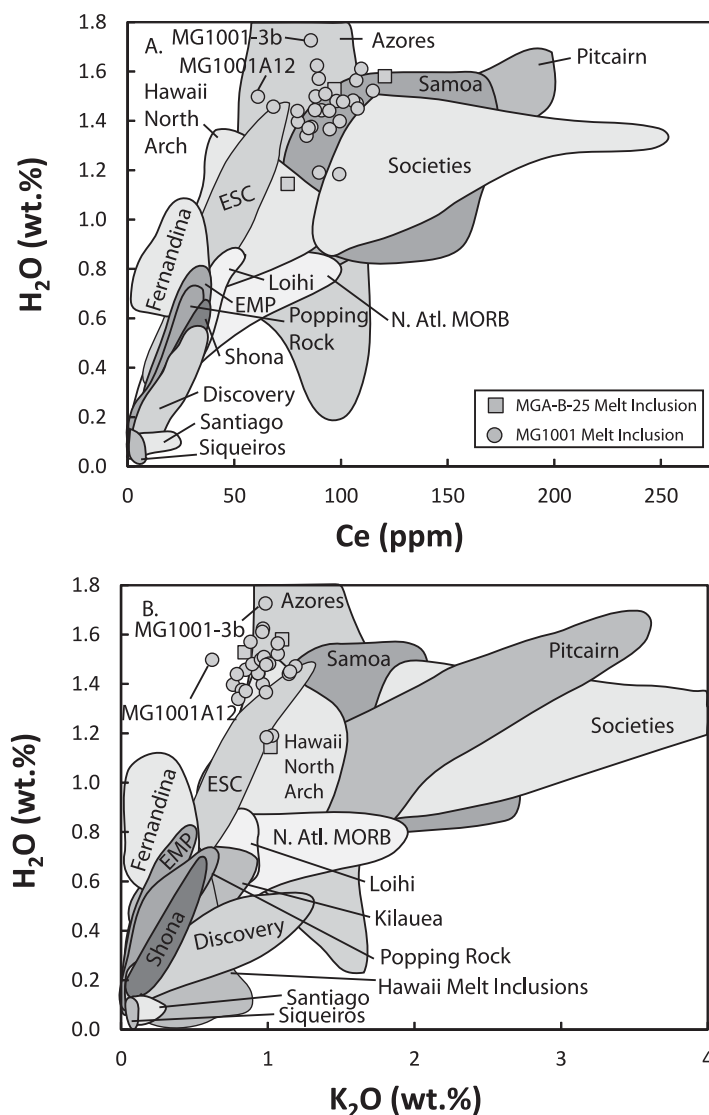
Figure 10. H_2O versus Ce and K_2O compared to global OIB and MORB data. Mangaia melt inclusion data are plotted as gray symbols following previous figure formatting, and have been corrected to be in equilibrium with the host olivine (supporting information Table S5). The H_2O contents found in Mangaia melt inclusions are among the highest for OIBs and MORBs. Data arrays from other OIB and MORB localities are plotted for comparison and consist of data collected from submarine glasses and melt inclusions [*Schilling et al.*, 1985; *Clague et al.*, 1995; *Douglass et al.*, 1995; *Dixon et al.*, 1997; *Langmuir et al.*, 1997; *Pan and Batiza*, 1998; *Dixon and Clague*, 2001; *Dixon et al.*, 2002; *Hauri*, 2002; *Kingsley*, 2002; *Saal et al.*, 2002; *Simons et al.*, 2002; *Yang et al.*, 2003; *le Roux et al.*, 2002; *Workman et al.*, 2004, 2006; *Cartigny et al.*, 2008, and references therein; *Koleszar et al.*, 2009; *Kelley et al.*, 2013; *Kendrick et al.*, 2014; *Metrich et al.*, 2014]. Easter microplate (EMP) and Easter seamount chain (ESC) are abbreviated for clarity. Kilauea glass and Hawaii melt inclusion samples [*Clague et al.*, 1995; *Hauri*, 2002] do not have trace element data and therefore do not plot in the H_2O versus Ce plot. The volatiles database was filtered in the same way as described in the caption of Figure 4.

submarine glasses and melt inclusions in the global OIB and MORB data set, but have intermediate Ce and K_2O concentrations; lavas erupted at EM1 and EM2 localities also tend to have elevated H_2O, but have higher Ce and K_2O at a given H_2O abundance. Lavas from the enriched mantle hot spots, which host elevated $^{87}Sr/^{86}Sr$ and lower $^{143}Nd/^{144}Nd$ ratios [*Zindler and Hart*, 1986; *Hofmann*, 1997], exhibit Ce concentrations that are nearly 2 times higher at a given H_2O abundance than the HIMU melts.

Plots of H_2O/Ce versus Sr and Pb isotopes also show fields for a number of OIB and MORB localities (Figure 11). Mangaia lavas and melt inclusions anchor the low $^{207}Pb/^{206}Pb$ and low $^{208}Pb/^{206}Pb$ region of the global data set, and in situ SIMS measurements of Pb isotopes on the Mangaia melt inclusions from this study have relatively homogeneous compositions that are similar to whole rocks from the island [*Nakamura and Tatsumoto*, 1988; *Dupuy et al.*, 1989; *Hauri and Hart*, 1993; *Woodhead*, 1996; *Kogiso et al.*, 1997; *Tatsumi et al.*, 2000; *Schiano et al.*, 2001; *Hanyu et al.*, 2011]. ESC lavas with the most radiogenic Pb-isotopic compositions ($^{206}Pb/^{204}Pb$, $^{207}Pb/^{204}Pb$, and $^{208}Pb/^{204}Pb$ up to 19.91, 15.64, and 39.66, respectively, which translates to $^{208}Pb/^{206}Pb = 1.99$ and $^{207}Pb/^{206}Pb = 0.785$) have

H_2O/Ce ratios (up to 244) that are similar to the highest H_2O/Ce ratios (~200) in the subset of Mangaia melt inclusions that show no evidence for assimilation. We note that other localities have even higher H_2O/Ce, including Pico Island in the Azores ($H_2O/Ce = 340$) [*Metrich et al.*, 2014] and N. Atlantic MORB (350) [*Dixon et al.*, 2002], which indicates that the HIMU mantle reservoir does not have the highest H_2O/Ce.

We note that *Dixon et al.* [2002] argued for a lower H_2O/Ce ratio for the HIMU mantle of 100, but this is a factor of two lower than the highest H_2O/Ce values from the ESC lavas with the most radiogenic Pb-isotopic compositions [*Dixon et al.*, 2002] and the Mangaia inclusions (~200). In contrast to the HIMU mantle, $H_2O/$

Ce values for EM-type (high $^{87}Sr/^{86}Sr$) lavas from Societies, Pitcairn, and Samoa extend to the low H_2O/Ce ratios ($H_2O/Ce < 100$) [*Dixon et al.*, 2002; *Workman et al.*, 2006; *Kendrick et al.*, 2014]. Thus, the EM mantle signature anchors the high $^{87}Sr/^{86}Sr$, low H_2O/Ce portion of the global mantle array. Sr-isotopes were not measured on the Mangaia inclusions, but if the Sr-isotopic compositions of the inclusions are similar to whole rocks from the island (just as Pb-isotopic compositions of the inclusion suite examined here are similar to the Pb-isotopic compositions of the whole rocks from Mangaia), then Mangaia, together with the ESC lavas with the most radiogenic Pb-isotopic ratios, anchors the low $^{87}Sr/^{86}Sr$ and high H_2O/Ce portion of the global mantle array.
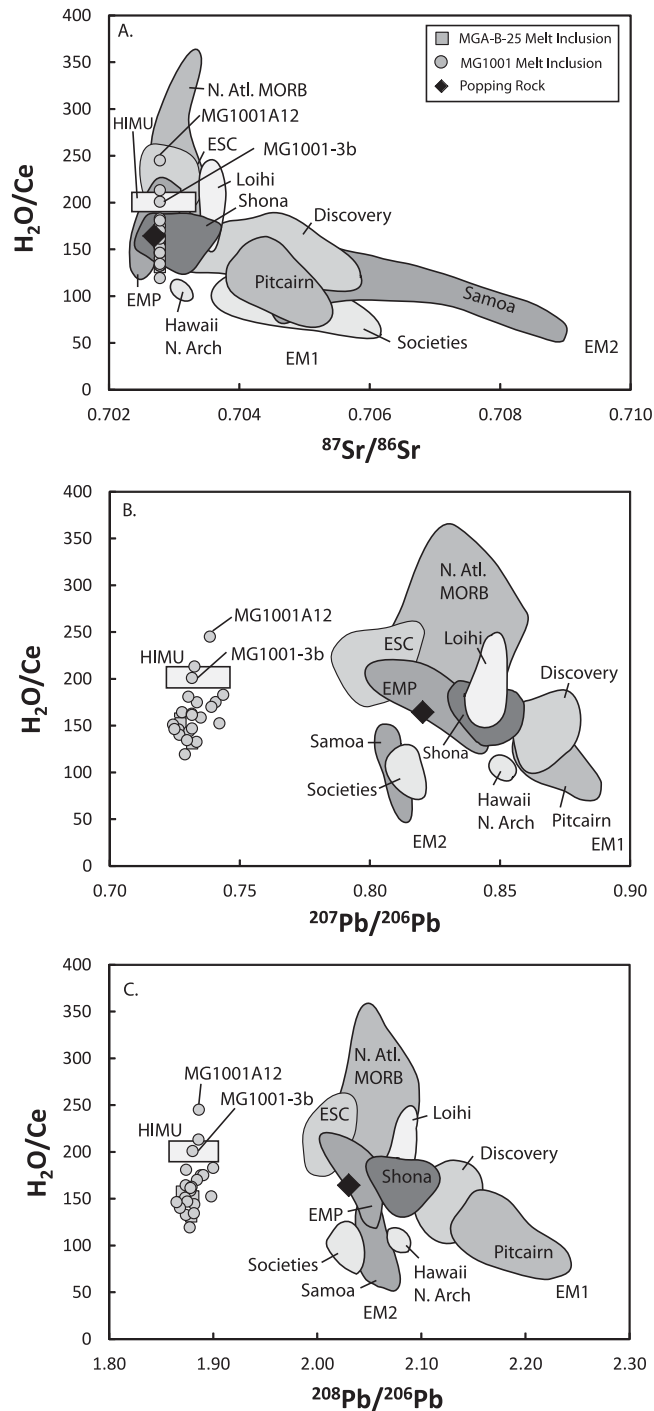
Given a H_2O/Ce ratio of the HIMU mantle of $\sim$200, it is possible to calculate the H_2O concentration of this mantle end-member if a reliable estimate for the mantle source Ce can be obtained. There are some bounds that can be placed on the Ce concentration of the HIMU mantle that can be used to constrain the H_2O abundance in the HIMU mantle source. It is important to note that the Ce concentrations for the HIMU mantle source are not known, and there are many uncertainties associated with estimating the abundances of incompatible elements in the mantle source of lavas. The following discussion uses estimates from the literature, and assumes that the HIMU mantle is a mixture of altered oceanic crust [*Hoffman and White*, 1982] and a depleted plume component, which is similar to earlier models for this mantle source [*Hauri and Hart*, 1993; *Stracke et al.*, 2003]. It is reasonable to assume that the Ce concentration will not be more depleted than the depleted plume component, which is estimated to have a Ce concentration of 1.3 ppm [*Jackson and Jellinek*, 2013], but not more enriched than altered oceanic crust, which is estimated to have a Ce concentration of 6 ppm (as provided by *Dixon et al.* [2002]). The proportion of the two end-members (altered oceanic crust and depleted plume component) contributing to the HIMU mantle source is estimated from prior work suggesting a two-component mixture for generating the HIMU Mangaia mantle source [e.g., *Hauri and Hart*, 1993]. If we assume the Mangaia HIMU mantle has a $\sim$20% contribution of recycled oceanic crust, which is consistent with coupled Os-isotopic and Pb-isotopic constraints on Mangaia lavas [*Hauri and Hart*, 1993], and if the remaining 80% of the Mangaia source is composed of the depleted plume component, then the Mangaia HIMU source has a Ce concentration of 2.2 ppm. Isotopic constraints suggest that higher proportions of recycled oceanic crust in the HIMU source are unlikely, particularly if the Mangaia mantle source is >2.5 Ga [*Hauri and Hart*, 1993; *Day et al.*, 2009, 2010]. *Dixon et al.* [2002] assumed a Ce concentration of 6 ppm for the HIMU source, which assumes that HIMU is pure recycled altered oceanic crust without a depleted mantle contribution; other estimates for the Ce concentration of altered oceanic crust and MORB are available in the literature [*Kelley et al.*, 2003; *Gale et al.*, 2013], but we use the estimate from *Dixon et al.* [2002] for direct comparison with their model results exploring the H_2O abundances in the mantle. We emphasize that the bulk major element composition of HIMU lavas, and the compositions of the olivines, are not well matched by melting a source comprised of purely mafic material [*Jackson and Dasgupta*, 2008; *Herzberg et al.*, 2014], and we do not advocate a model for the melting of a purely mafic lithology in the Mangaia mantle; instead, *Herzberg et al.* [2014] argue that the HIMU mantle consists of fertile peridotite enriched by mixing completely with a minor component of pyroxenite. Similarly, the contribution of 20% mafic material to the HIMU source is assumed to be mixed with the depleted-mantle peridotite such that the final mixture is an enriched peridotite [*Herzberg*, 2011]. Using the estimated H_2O/Ce ratio for Mangaia primary melts ($\sim$200), and a Ce concentration of 2.2 ppm, the H_2O concentration in the HIMU mantle source is estimated to be 440 ppm.

The primary uncertainty in the estimate of H_2O concentration of the HIMU source derives from uncertainty in the source Ce concentration, which in our calculation scales with the amount of recycled oceanic crust in the HIMU mantle. We have adopted a recycled oceanic crust mass fraction of 20% in our calculation based on isotopic constraints: a higher proportion of recycled oceanic crust will yield a higher estimated Ce concentration and a higher HIMU source H_2O concentration, and a lower proportion of oceanic crust yields a lower HIMU source H_2O concentration.

Using a simple melt model, a HIMU mantle source water content of 440 ppm can easily generate the H_2O abundances estimated for Mangaia primary melts. Following olivine fractionation correction so that the melt is in equilibrium with mantle olivine (Fo_{90}), the inclusion with the highest H_2O abundance (MG1001-3b

Figure 11. H_2O/Ce versus $^{87}Sr/^{86}Sr$, $^{207}Pb/^{206}Pb$, and $^{208}Pb/^{206}Pb$ isotopes for Mangaia melt inclusions and global OIBs and MORBs. The Pb-isotopic data for the Mangaia inclusions (supporting information Table S5) are relatively homogeneous and similar to Mangaia whole rock values. Therefore, while Sr-isotopes were not measured in the inclusions, they are also assumed to be homogeneous and similar to the Mangaia whole rock values. (a) We applied an average $^{87}Sr/^{86}Sr$ to all of the melt inclusions using data from *Hanyu et al.* [2011] for age corrected, leached whole rocks. Data from other OIB and MORB sources are provided for comparison and consist of submarine glass samples and melt inclusions [*Staudigel et al.*, 1984; *Hannan and Schilling*, 1989; *Devey et al.*, 1990; *Dosso et al.*, 1991; *Fontignie and Schilling*, 1991; *Woodhead and Devey*, 1993; *Douglass et al.*, 1995; *Dixon et al.*, 1997; *Kingsley and Schilling*, 1998; *Douglass et al.*, 1999; *Dosso et al.*, 1999; *Frey et al.*, 2000; *Dixon and Clague*, 2001; *Dixon et al.*, 2002; *Kingsley*, 2002; *Simons et al.*, 2002; *Yang et al.*, 2003; *Honda and Woodhead*, 2005; *Workman et al.*, 2006; *Cartigny et al.*, 2008, and references therein; *Hanyu et al.*, 2011; *Kelley et al.*, 2013; *Kendrick et al.*, 2013a, 2014]. Not all data from Figure 10 are shown in this figure because isotopic compositions are not available. The box labeled "HIMU" is the estimated range of the HIMU source value, and excludes the Mangaia inclusion with the highest H_2O/Ce (245; inclusion MG1001A12) owing to possible assimilation of seawater or altered oceanic crust. The volatiles database was filtered in the same way as described in the caption of Figure 4.

has 1.73 wt % H_2O, when corrected to be in equilibrium with the host olivine; supporting information Table S5) has a water concentration of 1.37 wt % (and an H_2O/Ce ratio of ~200). Using mineral-melt partition coefficients and a mantle source mineralogy with clinopyroxene (12% modal abundance), orthopyroxene (25%), olivine (55%), and garnet (8%) modes provided in *Kelemen et al.* [2004] and summarized in *Jackson et al.* [2010], and assuming that H_2O and Ce have the same mineral-melt partition coefficients during mantle melting, we use a modal aggregated fractional melting model to explore the conditions under which a mantle source with 440 ppm H_2O can generate melts with 1.37 wt % H_2O.

If the HIMU source has 440 ppm H_2O, then the water abundance of the HIMU primary melt (1.37 wt %) is achieved when the melt fraction is 3.0%. This degree of melting is within the range previously suggested for melt generation in the Cook-Australs [*Herzberg and Gazel*, 2009].

The melt model can also be used to provide an estimate of the refractory lithophile element concentrations in the Mangaia mantle source. When the melt fraction is ~3%, the melt model yields a Ce concentration of 68.5 ppm in the melt (assuming 2.2 ppm Ce in the HIMU source). This value is identical to the Ce concentration (68.5 ppm) for the inclusion with the highest H_2O (MG1001-3b) following olivine fractionation correction so that the melt is in equilibrium with mantle olivine (Fo_{90}), and this trace element composition is adopted as the Mangaia primary melt composition (see Figure 3 caption). Because the melt model does a reasonable job of matching the Ce concentration in Mangaia primary melts, we use the same melt model (with ~3% melting), together with the estimated Mangaia primary melt trace element composition, to invert for the source composition of the other trace elements in the primary melt shown in Figure 3 (and presented in the caption). Using the specified melt model, this source will generate the trace element abundances in the Mangaia primary melt composition when the melt fraction is ~3%. This source composition is presented in the caption of Figure 3.

4.3. Dehydration of the Subducted Slab to Generate the HIMU Source

Altered oceanic crust is estimated to have a H_2O/Ce ratio of 2500–5000 [*Dixon et al.*, 2002] and a water concentration of 2–3 wt %. If the HIMU mantle hosts a significant component of recycled oceanic crust, then an important question remains: How did the H_2O/Ce ratio become so low in the HIMU mantle? Subducted material experiences a two-stage dehydration process: (1) stage one is defined by subduction zone processing [e.g., *Hacker*, 2008; *van Keken et al.*, 2011], where H_2O is lost from the slab, and (2) stage two is defined by diffusion of water out of the subducted slab during long-term storage in the mantle [e.g., *Workman et al.*, 2006]. Following *Dixon et al.* [2002], we can look at the net effect of these two processes by comparing presubduction H_2O/Ce ratios of mature oceanic crust to the H_2O/Ce ratios in HIMU melt inclusions erupted at Mangaia. Compared to the presubduction mature oceanic crust H_2O/Ce of 2500–5000, we find that the HIMU mantle source today, which is suggested to be a mixture of recycled material and depleted plume component mantle [e.g., *Hauri and Hart*, 1993], has an H_2O/Ce ratio of ~200 (which is a factor of two higher than the H_2O/Ce ratio suggested for the HIMU source [~100] by *Dixon et al.* [2002]). A reduction of the H_2O/Ce ratio from 2500–5000 to 200 represents a factor of 12.5–25 reduction in original H_2O content in the subducted slab compared to the loss of Ce.

It is useful to deconvolve the relative effects of stage one of dehydration (subduction zone processing) from the effects of stage two of dehydration (long-term mantle storage, diffusive water loss). *van Keken et al.* [2011] reported estimates of water content entering subduction zones and surviving to reach >230 km depth based on petrological models and global subduction zone rock fluxes. Using H_2O values of igneous crust from before subduction (9.3×10^8 Tg/Myr) [*Hacker*, 2008] and after subduction (1.8×10^8 Tg/Myr) [*van Keken*, 2011], igneous crust is estimated to dehydrate 81% from the subduction process alone. This constrains long-term storage dehydration of the slab by diffusive water loss to account for the remaining reduction of water in the HIMU mantle reservoir, which can efficiently reduce H_2O contents in subducted slabs on geologic time scales (see below).

Diffusion rates for trace elements (like Ce) are very low and heterogeneities in the solid mantle will not equilibrate with these elements on length scales of more than 10 m over the age of the Earth [e.g., *Hofmann and Hart*, 1978; *Van Orman et al.*, 2001]. In contrast, hydrogen diffuses quickly and the H_2O/Ce ratio can be reduced by diffusive loss of H_2O into the ambient mantle. Using the H_2O concentration values of altered oceanic crust from *Dixon et al.* [2002] (2–3 wt %) and the amount of dehydration calculated above (81%), the recycled slab after the subduction zone would have 0.38–0.57 wt % (3800–5700 ppm) H_2O. If the

Mangaia mantle, which is estimated to have 440 ppm water, is composed of recycled slab (20% by mass) and a depleted component (80%) that has a water content similar to ambient mantle (116 ppm) [*Salters and Stracke*, 2004], then the slab component in the Mangaia mantle has a water content of ~1740 ppm. This is 2.2–3.3 times lower than the estimated water content of a slab subducted to postarc depths, and we argue that diffusive loss from the slab during long-term storage in the mantle can reduce the water content in the slab from postsubduction values.

We model the effect of diffusion in a manner similar to *Workman et al.* [2006]. A diffusion calculation [see *Zhang*, 2008, equation (3-48b)] was performed assuming the placement of postsubduction mature oceanic crust in an infinite reservoir of depleted mantle. We estimate depleted mantle to have 116 ppm H_2O [*Salters and Stracke*, 2004], adopt a thickness of 7 km for the slab, and assume a storage time of 2.5 Ga. The range of water contents remaining in the slab after subduction (0.38–0.57 wt % H_2O) are used as inputs for the diffusion calculation. The diffusion coefficient of H in olivine was found to be 1.4×10^{-8} m^2/s at 1600°C for the [100] (fast) axis by *Mackwell and Kohlstedt* [1990]. In this simple diffusion calculation, following subduction, the slab experiences approximately 90% diffusive loss of water during 2.5 Ga of residence in the mantle: the water content of the slab is reduced from 3800 to 5700 ppm to approximately 340 to 450 ppm. Thus, diffusive loss of H_2O from the slab following subduction zone dehydration would make the slab much drier (340–450 ppm H_2O) than our model for the slab (1740 ppm H_2O) in the HIMU mantle. However, if the slab is thicker, or slabs pile up on each other in the mantle (effectively thickening the diffusive distance), then the diffusive loss of H_2O would be reduced. Additionally, we note that pyroxene-rich and garnet-rich lithologies have a higher water storage capacity than olivine-rich lithologies [*Hirschmann et al.*, 2009; *O'Leary et al.*, 2010; *Ardia et al.*, 2012], and higher modal pyroxene and garnet abundances in the HIMU mantle source may allow the preservation of higher water abundances during long-term storage in the mantle. This is not an unreasonable model, as HIMU sources have long been suggested to host a significant mafic component [*Hofmann and White*, 1982; *Hauri and Hart*, 1993; *Day et al.*, 2009] or to be a fertile peridotite that has been enriched by mixing completely with a component of pyroxenite (thereby increasing the pyroxene abundance in the enriched peridotite resulting from the mixture) [*Herzberg et al.*, 2014].

4.4. CO_2 in the Generation of HIMU Lavas

It is apparent that the CO_2 concentrations in Mangaia melt inclusions are high compared to CO_2 abundances measured in many other OIB settings (Figure 4b). In fact, carbonate blebs were previously noted in crystalline melt inclusions hosted in olivines [*Saal et al.*, 1998; *Yurimoto et al.*, 2004], and *Saal et al.* [1998] found that melt inclusions from two of the whole rocks (MGA-B-47 and MGA-B-25) examined in this study host carbonatite blebs (unfortunately, we did not examine these particular melt inclusions). We infer that some inclusions in the present study may have also hosted carbonate blebs prior to homogenization, but we did not observe carbonatite blebs in the inclusions posthomogenization. *Saal et al.* [1998] suggested that carbonatite plays a key role in the genesis of HIMU lavas, and *Hauri et al.* [1993] found that carbonatite plays an important role in modifying mantle xenoliths from the island of Tubuai (located in the Cook-Australs). The association of carbonate with lavas derived from the HIMU mantle source could be an important clue for ultimately understanding the origin of this mantle end-member [*Jackson and Dasgupta*, 2008].

Partial melt compositions of carbonated mafic lithologies are shown experimentally to give rise to melts that are similar to the inferred compositions of HIMU primary melts (matching geochemical characteristics such as SiO_2, TiO_2, Al_2O_3, CaO, Na_2O, and CaO/Al_2O_3) [*Dasgupta et al.*, 2004; *Gerbode and Dasgupta*, 2010; *Mallik and Dasgupta*, 2012]. It has also been suggested that there is interaction of this melt product with surrounding peridotite, which leads to a closer match for FeO and is consistent with a recent study of the HIMU mantle source lithology by *Herzberg et al.* [2014] [*Dasgupta et al.*, 2004; *Gerbode and Dasgupta*, 2010; *Mallik and Dasgupta*, 2012]. Experimental evidence shows that it is difficult to generate strongly SiO_2-undersaturated and high CaO/Al_2O_3 melt compositions, like those observed in HIMU lavas, without high concentrations of CO_2 in the mantle source [*Kushiro*, 1975; *Eggler*, 1978; *Dasgupta et al.*, 2004, 2007; *Gerbode and Dasgupta*, 2010; *Mallik and Dasgupta*, 2012], which strongly suggests that the HIMU mantle end-member is CO_2-rich.

Unfortunately, it is not possible to reliably estimate the CO_2 abundance in the primary melts of the HIMU mantle owing to large uncertainties in the CO_2/Nb ratio that has been used to estimate mantle source CO_2 abundances [*Saal et al.*, 2002]. The CO_2/Nb ratio of the depleted mantle is estimated to be 300 [*Koleszar*

et al., 2009], which is slightly higher than the value of 239 that was originally proposed [*Saal et al.*, 2002], and this is likely a lower limit for the CO_2/Nb ratio of the OIB mantle. *Cartigny et al.* [2008] observed a relationship between CO_2/Nb and $(La/Sm)_N$ in MORB. If we assume that this relationship applies to the Mangaia melts, which have an average $(La/Sm)_N$ of 2.9 (supporting information Table S5), then the CO_2/Nb of the Mangaia mantle source is ~1000; this value, when paired with the estimated Nb concentration of the HIMU mantle source (see caption of Figure 3), yields unreasonably high CO_2 in Mangaia primary melts. If carbonatite is present during melting, CO_2 and Nb will have dramatically different partition coefficients, and CO_2/Nb ratios in the primary melt will exceed 10^4 [*Dasgupta et al.*, 2009]. This serves to underscore the great uncertainty in the CO_2/Nb ratio of primary melts, particularly when carbonatite is present.

While it is not possible to reliably estimate the CO_2 in abundance in the HIMU mantle source or in HIMU primary melts, the HIMU mantle is thought to have elevated CO_2 [*Hauri et al.*, 1993; *Saal et al.*, 1998; *Jackson and Dasgupta*, 2008; *Castillo*, 2014]. The origin of this elevated CO_2 may be traced to the recycled crustal origin of the HIMU mantle, where CO_2-rich and H_2O-rich altered oceanic crust [e.g., *Staudigel et al.*, 1996; *Alt and Teagle*, 1999; *Bach et al.*, 2001; *Wallmann*, 2001; *Dixon et al.*, 2002; *Gillis and Coogan*, 2011] is subducted into the mantle and recycled into the origin of HIMU lavas. The carbonated nature of the HIMU mantle source is consistent with experimental work attempting to model the major element composition of HIMU lavas [*Dasgupta et al.*, 2004; *Gerbode and Dasgupta*, 2010; *Mallik and Dasgupta*, 2012] and has important implications for the deep storage of recycled carbon in the mantle.

4.5. F/Nd and Cl/Nb Signature of HIMU Melts

The F and Cl concentrations in melt inclusions are useful for constraining the undegassed, preeruptive compositions because their degassing pressure is typically less than 100 bars [*Spilliaert et al.*, 2006]. Additionally, F and Cl are not thought to diffuse in or out of the host olivine [*Bucholz et al.*, 2013]. Normalizing F and Cl to elements with similar bulk partition coefficients, namely Nd and Nb, respectively [*Dalou*, 2011], the F/Nd and Cl/Nb ratios measured in melt inclusions have been used to characterize those of the source [e.g., *Rose-Koga et al.*, 2012]. Known as a canonical ratio, F/Nd is largely insensitive to mantle melting, and natural samples (melt inclusions and glasses from MORB and OIB) display a relatively constant value of 21 over a range of Nd concentrations that vary over two orders of magnitude [*Workman et al.*, 2006]. In cases where a melt inclusion has undergone assimilation of crustal materials or brines, F/Nd as high as 60–183 have been observed [*Lassiter et al.*, 2002]. However, such inclusions are often accompanied by extremely elevated Cl/Nb ratios (from 1271 to 7166; see section 2) [*Lassiter et al.*, 2002]. Typically, Cl/Nb ranges from 5 to 35 among the data of MORB and OIB glasses and melt inclusions [*Lassiter et al.*, 2002; *Saal et al.*, 2002; *Workman et al.*, 2006; *Koleszar et al.*, 2009; *Shaw et al.*, 2010; *Kendrick et al.*, 2014; *Metrich et al.*, 2014; www.earthchem.org/petdb]. Notably, once altered oceanic crust assimilation has been identified and excluded, any deviation from the relatively small range of these geochemical ratios indicates the presence of material that is not considered to be typical mantle.

Mangaia melt inclusions display Cl/Nb values similar to MORB melt inclusions and samples from other OIBs, such as the Azores and Samoa (Figure 7). The Cl/Nb ratio of the source of Mangaia is likely similar to that of the MORB source. On the contrary, Mangaia melt inclusions show a higher F/Nd (30 ± 9; 2σ standard deviation) than the "MORB-OIB" canonical value of 21, and the Mangaia inclusions range up to a F/Nd ratio of 41. The higher F/Nd values are mainly related to higher F concentrations in the Mangaia melt inclusions (about 30% higher), while Nd concentrations are comparable to other OIB data (e.g., 45 ± 5 ppm; the Azores, Samoa, and this study). The Nd concentration in the HIMU source is estimated to be 1.38 ppm (see Figure 3), which, when combined with the average Mangaia melt inclusion F/Nd ratio (30), yields F abundances in the HIMU source of 41 ppm. By comparison, the F concentrations of DMM and chondrite-based primitive mantle are estimated to be 11 and 25 ppm, respectively [*McDonough and Sun*, 1995; *Salters and Stracke*, 2004].

The recycled HIMU component with high H_2O and CO_2 is also inferred to have high F. While F and Cl are likely elevated in the subducting slab, most of the subduction input is expected to be stripped off during prograde dehydration, as reflected in elevated F and Cl concentrations in many arc magmas and forearc serpentines [e.g., *Straub and Layne*, 2003; *John et al.*, 2011; *Rose-Koga et al.*, 2012; *Kendrick et al.*, 2013b; *Debret et al.*, 2014]. The data from Mangaia melt inclusions suggest that the recycled component in the HIMU source is characterized by the fractionation of F from Cl, as Mangaia samples have Cl/Nb ratios similar to ambient mantle, while F/Nd and H_2O/Ce ratios remain higher than ambient mantle. However, the precise

mechanism responsible for fractionation of F and H_2O from Cl in subduction zones is not well known. The hydroxyl site in silicate minerals—which has a strong affinity for F [e.g., *Smith*, 1981; *Smith et al.*, 1981; *Wu and Koga*, 2013]—provides an ideal mineralogical site to promote recycling of H_2O and F, but not Cl. Thus, the residual mineralogy of the subducted slab after it has gone through prograde dehydration/melting, including phlogopite, humite, apatite, and/or amphiboles (together with their high pressure polymorphs), will play an important role in the fractionation of H_2O and F from Cl [*Rose-Koga et al.*, 2014].

5. Conclusions

Pb-isotopic studies of lavas from Mangaia have established this locality to be the surface expression of the HIMU mantle end-member, which has long been considered to contain subducted oceanic crust in the mantle source [*Hofmann and White*, 1982; *Zindler and Hart*, 1986; *Hauri and Hart*, 1993; *Kelley et al.*, 2005; *Hanyu et al.*, 2011]. Sulfur isotopic work on melt inclusions from the island has established that the material erupted at Mangaia was once at the Earth's surface > 2.45 Ga, confirming the recycled origin hypothesis for the HIMU mantle [*Cabral et al.*, 2013].

Previous work on HIMU melt inclusions has been restricted to the study of crystalline inclusions from Mangaia [*Saal et al.*, 1998; *Yurimoto et al.*, 2004; *Paul et al.*, 2011], which cannot be used to measure volatile abundances. Additionally, because of the lack of dredging expeditions to this location, the scientific community has been without glasses from Mangaia on which to perform volatile measurements. Here, we have homogenized crystalline melt inclusions hosted in olivine phenocrysts from the island. We have performed in situ volatile, trace, and major element analyses in the melt inclusions, in addition to in situ Pb-isotopic analyses. We find Mangaia melt inclusions host elevated H_2O (up to 1.73 wt %) and CO_2 (up to 2346 ppm) contents.

We suggest that the H_2O abundance in the HIMU mantle source is ~440 ppm, which can generate the H_2O abundance observed in the melt inclusion with the highest H_2O concentration when the melt fraction is ~3%. The inclusions have relatively high concentrations of CO_2 (up to 2346 ppm), which is consistent with previous observations of carbonatite in Mangaia melt inclusions. The high levels of CO_2 in HIMU lavas, and hence the HIMU mantle source, are consistent with the experimental studies that require a carbonated protolith to generate the unique major element composition of the melts.

We also find the F/Nd ratios of the melt inclusions (30 ± 9; 2σ standard deviation) to be higher than the canonical value (21), while Cl/Nb ratios in Mangaia inclusions are likely similar to the MORB mantle. We suggest that this may owe to the influence of hydroxyl sites in silicate minerals, which may promote recycling of H_2O and F, but not Cl.

References

Allègre, C. J. (1982), Chemical geodynamics, *Tectonophysics*, *81*, 109–132.

Alt, J. C., and D. A. H. Teagle (1999), The uptake of carbon during alteration of ocean crust, *Geochim. Cosmochim. Acta*, *63*, 1527–1535.

Ardia, P., M. M. Hirschmann, A. C. Withers, and T. J. Tenner (2012), H_2O storage capacity of olivine at 5–8GPa and consequences for dehydration partial melting of the upper mantle, *Earth Planet. Sci. Lett.*, *345–348*, 104–116, doi:10.1016/j.epsl.2012.05.038.

Asimow, P. D., and C. H. Langmuir (2003), The importance of water to oceanic mantle melting regimes, *Nature*, *421*, 815–820.

Bach, W., J. C. Alt, Y. Niu, S. E. Humphris, J. Erzinger, and H. J. B. Dick (2001), The geochemical consequences of late-stage low-grade alteration of lower ocean crust at the SW Indian Ridge: Results from ODP Hole 735B (Leg 176), *Geochim. Cosmochim. Acta*, *65*, 3267–3287.

Bucholz, C. E., G. A. Gaetani, M. D. Behn, and N. Shimizu (2013), Post-entrapment modification of volatiles and oxygen fugacity in olivine-hosted melt inclusions, *Earth Planet. Sci. Lett.*, *374*, 145–155, doi:10.1016/j.epsl.2013.05.033.

Cabral, R. A., M. G. Jackson, E. F. Rose-Koga, K. T. Koga, M. J. Whitehouse, M. A. Antonelli, J. Farquhar, J. M. D. Day, and E. H. Hauri (2013), Anomalous sulphur isotopes in plume lavas reveal deep mantle storage of Archaean crust, *Nature*, *496*, 490–493, doi:10.1038/nature12020.

Cartigny, P., F. Pineau, C. Aubaud, and M. Javoy (2008), Towards a consistent mantle carbon flux estimate: Insights from volatile systematics (H_2O/Ce, δD, CO_2/Nb) in the North Atlantic mantle (14° N and 34° N), *Earth Planet. Sci. Lett.*, *265*, 672–685, doi:10.1016/j.epsl.2007.11.011.

Castillo, P. R. (2014), Recycling of marine carbonate as a possible solution to the Pb paradox, *Mineral. Mag.*, 358.

Chan, L.-H., J. C. Lassiter, E. H. Hauri, S. R. Hart, and J. Blusztajn (2009), Lithium isotope systematics of lavas from the Cook-Austral Islands: Constraints on the origin of HIMU mantle, *Earth Planet. Sci. Lett.*, *277*, 433–442, doi:10.1016/j.epsl.2008.11.009.

Chase, C. G. (1981), Oceanic island Pb: Two-stage histories and mantle evolution, *Earth Planet. Sci. Lett.*, *52*, 277–284.

Chauvel, C., A. Hofmann, and P. Vidal (1992), HIMU-EM: The French Polynesian connection, *Earth Planet. Sci. Lett.*, *110*, 99–119.

Chauvel, C., W. McDonough, G. Guille, R. Maury, and R. Duncan (1997), Contrasting old and young volcanism in Rurutu Island, Austral chain, *Chem. Geol.*, *139*, 125–143.

Chen, Y., A. Provost, P. Schiano, and N. Cluzel (2011), The rate of water loss from olivine-hosted melt inclusions, *Contrib. Mineral. Petrol.*, *162*(3), 625–636, doi:10.1007/s00410-011-0616-5.

Cherniak, D. J. (2010), Diffusion in accessory minerals: Zircon, titanite, apatite, monazite and xenotime, *Rev. Mineral. Geochem.*, *72*(1), 827–869, doi:10.2138/rmg.2010.72.18.

Clague, D. A., J. G. Moore, J. E. Dixon, and W. B. Friesen (1995), Petrology of submarine lavas from Kilauea's Puna Ridge, Hawaii, *J. Petrol.*, *36*, 299–349.

Cohen, R. S., and R. K. O'Nions (1982), Identification of recycled continental material in the mantle from Sr, Nd and Pb isotope investigations, *Earth Planet. Sci. Lett.*, *61*, 73–84.

Dalou, C. (2011), Fluorine and chlorine fractionation in the sub-arc mantle: An experimental investigation, thesis, Univ. Blaise Pascal, Clermont-Ferrand, France.

Danyushevsky, L. V., A. V. Sobolev, and N. N. Kononkova (1992), Methods of studying melt inclusions in minerals during investigations on water-bearing primitive mantle melts (Tonga Trench boninites), *Geochem. Int.*, *29*, 48–62.

Danyushevsky, L. V., F. N. Della-Pasqua, and S. Sokolov (2000), Re-equilibration of melt inclusions trapped by magnesian olivine phenocrysts from subduction-related magmas: Petrological implications, *Contrib. Mineral. Petrol.*, *138*, 68–83.

Dasgupta, R., M. M. Hirschmann, and A. C. Withers (2004), Deep global cycling of carbon constrained by the solidus of anhydrous, carbonated eclogite under upper mantle conditions, *Earth Planet. Sci. Lett.*, *227*, 73–85, doi:10.1016/j.epsl.2004.08.004.

Dasgupta, R., M. M. Hirschmann, and N. D. Smith (2007), Partial melting experiments of peridotite + CO_2 at 3 GPa and genesis of Alkalic Ocean Island Basalts, *J. Petrol.*, *48*(11), 2093–2124, doi:10.1093/petrology/egm053.

Dasgupta, R., M. M. Hirschmann, W. F. McDonough, M. Spiegelman, and A. C. Withers (2009), Trace element partitioning between garnet lherzolite and carbonatite at 6.6 and 8.6 GPa with applications to the geochemistry of the mantle and of mantle-derived melts, *Chem. Geol.*, *262*, 57–77, doi:10.1016/j.chemgeo.2009.02.004.

Day, J. M. D., D. G. Pearson, C. G. Macpherson, D. Lowry, and J.-C. Carracedo (2009), Pyroxenite-rich mantle formed by recycled oceanic lithosphere: Oxygen-osmium isotope evidence from Canary Island lavas, *Geology*, *37*(6), 555–558, doi:10.1130/G25613A.1.

Day, J. M. D., D. G. Pearson, C. G. Macpherson, D. Lowry, and J. C. Carracedo (2010), Evidence for distinct proportions of subducted oceanic crust and lithosphere in HIMU-type mantle beneath El Hierro and La Palma, Canary Islands, *Geochim. Cosmochim. Acta*, *74*(22), 6565–6589, doi:10.1016/j.gca.2010.08.021.

Debret, B., K. T. Koga, C. Nicollet, M. Andreani, and S. Schwartz (2014), F, Cl and S input via serpentinite in subduction zones: Implications for the nature of the fluid released at depth, *Terra Nova*, *26*(2), 96–101, doi:10.1111/ter.12074.

Devey, C. W., F. Albarede, J.-L. Cheminée, A. Michard, R. Mühe, and P. Stoffers (1990), Active submarine volcanism on the society hotspot swell (west Pacific): A geochemical study, *J. Geophys. Res.*, *95*, 5049–5066.

Dixon, J., D. A. Clague, P. Wallace, and R. Poreda (1997), Volatiles in alkalic basalts form the North Arch Volcanic Field, Hawaii: Extensive degassing of deep submarine-erupted alkalic series lavas, *J. Petrol.*, *38*(7), 911–939.

Dixon, J. E. (1997), Degassing of alkalic basalts, *Am. Mineral.*, *82*, 368–378.

Dixon, J. E., and D. A. Clague (2001), Volatiles in basaltic glasses from Loihi Seamount, Hawaii: Evidence for a relatively dry plume component, *J. Petrol.*, *42*, 627–654.

Dixon, J. E., L. Leist, C. Langmuir, and J.-G. Schilling (2002), Recycled dehydrated lithosphere observed in plume-influenced mid-ocean-ridge basalt, *Nature*, *420*, 385–389.

Dosso, L., B. B. Hanan, H. Bougault, J.-G. Schilling, and J.-L Joron (1991), Sr-Nd-Pb geochemical morphology between 10° and 17°N on the Mid-Atlantic Ridge: A new MORB isotope signature, *Earth Planet. Sci. Lett.*, *106*, 29–43.

Dosso, L., H. Bougault, C. Langmuir, C. Bollinger, O. Bonnier, and J. Etoubleau (1999), The age and distribution of mantle heterogeneity along the Mid-Atlantic Ridge (31–41°N), *Earth Planet. Sci. Lett.*, *170*, 269–286.

Douglass, J., J.-G. Schilling, and R. H. Kingsley (1995), Influence of the discovery and Shona mantle plumes on the southern Mid-Atlantic Ridge: Rare earth evidence, *Geophys. Res. Lett.*, *22*, 2893–2896.

Douglass, J., J.-G. Schilling, and D. Fontignie (1999), Plume-ridge interactions of the discovery and Shona mantle plumes with the southern Mid-Atlantic Ridge (40°–55°S), *J. Geophys. Res.*, *104*, 2941–2962.

Dupuy, C., H. G. Barsczus, J. Dostal, P. Vidal, and J.-M. Liotard (1989), Subducted and recycled lithosphere as the mantle source of ocean island basalts from southern Polynesia, central Pacific, *Chem. Geol.*, *77*, 1–18.

Eggler, D. (1978), The effect of CO_2 upon partial melting of peridotite in the system Na_2O-CaO-Al_2O_3-MgO-SiO_2-CO_2 to 35 Kb, with an analysis of melting in peridotite-H_2O-CO_2 system, *Am. J. Sci.*, *278*, 305–343.

Eiler, J. M., K. A. Farley, J. W. Valley, E. M. Stolper, E. H. Hauri, and H. Craig (1995), Oxygen isotope evidence against bulk recycled sediment in the mantle sources of Pitcairn Island lavas, *Nature*, *377*, 138–141.

Eisele, J., M. Sharma, S. J. G. Galer, J. Blichert-Toft, C. W. Devey, and A. W. Hofmann (2002), The role of sediment recycling in EM-1 inferred from Os, Pb, Hf, Nd, Sr isotope and trace element systematics of the Pitcairn hotspot, *Earth Planet. Sci. Lett.*, *196*, 197–212.

Fontignie, D., and J.-G. Schilling (1991), ^{87}Sr/^{86}Sr and REE variations along the Easter Microplate boundaries (south Pacific): Application of multivariate statistical analyses to ridge segmentation, *Chem. Geol.*, *89*, 209–241.

Frey, F. A., D. Clague, J. J. Mahoney, and J. M. Sinton (2000), Volcanism at the edge of the Hawaiian plume: Petrogenesis of submarine alkalic lavas from the North Arch volcanic field, *J. Petrol.*, *41*, 667–691.

Gaetani, G. A., and T. L. Grove (1998), The influence of water on melting of mantle peridotite, *Contrib. Mineral. Petrol.*, *131*, 323–346.

Gaetani, G. A., and E. B. Watson (2000), Open system behavior of olivine-hosted melt inclusions, *Earth Planet. Sci. Lett.*, *183*, 27–41.

Gaetani, G. A., J. A. O'Leary, N. Shimizu, C. E. Bucholz, and M. Newville (2012), Rapid reequilibration of H_2O and oxygen fugacity in olivine-hosted melt inclusions, *Geology*, *40*(10), 915–918, doi:10.1130/G32992.1.

Gale, A., M. Laubier, S. Escrig, and C. H. Langmuir (2013), Constraints on melting processes and plume-ridge interaction from comprehensive study of the FAMOUS and North Famous segments, Mid-Atlantic Ridge, *Earth Planet. Sci. Lett.*, *365*, 209–220, doi:10.1016/j.epsl.2013.01.022.

Gast, P. W., G. R. Tilton, and C. Hedge (1964), Isotopic composition of lead and strontium from Ascension and Gough Islands, *Science*, *145*, 1181–1185.

Gerbode, C., and R. Dasgupta (2010), Carbonate-fluxed melting of MORB-like pyroxenite at 2.9 GPa and genesis of HIMU Ocean Island Basalts, *J. Petrol.*, *51*(10), 2067–2088, doi:10.1093/petrology/egq049.

Gillis, K. M., and L. A. Coogan (2011), Secular variation in carbon uptake into the ocean crust, *Earth Planet. Sci. Lett.*, *302*, 385–392, doi:10.1016/j.epsl.2010.12.030.

Graham, D., S. Humphris, and W. Jenkins (1992), Helium isotope geochemistry of some volcanic rocks from Saint Helena, *Earth Planet. Sci. Lett.*, *110*, 121–131.

Hacker, B. R. (2008), H_2O subduction beyond arcs, *Geochem. Geophys. Geosyst.*, *9*, Q03001, doi:10.1029/2007GC001707.

Hanyu, T., and I. Kaneoka (1997), The uniform and low ^{3}He/^{4}He ratios of HIMU basalts as evidence for their origin as recycled materials, *Nature*, *390*, 273–276.

Hanyu, T., et al. (2011), Geochemical characteristics and origin of the HIMU reservoir: A possible mantle plume source in the lower mantle, *Geochem. Geophys. Geosyst.*, *12*, Q0AC09, doi:10.1029/2010GC003252.

Hanyu, T., et al. (2014), Isotope evolution in the HIMU reservoir beneath St. Helena: Implications for the mantle recycling of U and Th, *Geochim. Cosmochim. Acta*, *143*, 232–252, doi:10.1016/j.gca.2014.03.016.

Hart, S. (2011), The Mantle Zoo: New species, endangered species, extinct species, *Mineral. Mag.*, *3*, 983.

Hart, S., and H. Staudigel (1982), The control of alkalies and uranium in seawater by ocean crust alteration, *Earth Planet. Sci. Lett.*, *58*, 202–212.

Hart, S. R. (1988), Heterogeneous mantle domains: Signatures, genesis and mixing chronologies, *Earth Planet. Sci. Lett.*, *90*, 273–296.

Hart, S. R., E. H. Hauri, L. A. Oschmann, and J. A. Whitehead (1992), Mantle plumes and entrainment: Isotopic evidence, *Science*, *256*, 517–520.

Hauri, E. (2002), SIMS analysis of volatiles in silicate glasses. 2: Isotopes and abundances in Hawaiian melt inclusions, *Chem. Geol.*, *183*, 115–141.

Hauri, E. H., and S. R. Hart (1993), Re-Os isotope systematics of HIMU and EMII oceanic island basalts from the south Pacific Ocean, *Earth Planet. Sci. Lett.*, *114*, 353–371.

Hauri, E. H., and S. R. Hart (1997), Rhenium abundances and systematics in oceanic basalts, *Chem. Geol.*, *139*, 185–205.

Hauri, E., N. Shimizu, J. Dieu, and S. Hart (1993), Evidence for hotspot-related carbonatite metasomatism in the oceanic upper mantle, *Nature*, *365*, 221–227.

Hémond, C., C. Devey, and C. Chauvel (1994), Source compositions and melting processes in the Society and Austral plumes (South Pacific Ocean): Element and isotope (Sr, Nd, Pb, Th) geochemistry, *Chem. Geol.*, *115*, 7–45.

Herzberg, C. (2011), Identification of source lithology in the Hawaiian and Canary Islands: Implications for origins, *J. Petrol.*, *52*(1), 113–146, doi:10.1093/petrology/egq075.

Herzberg, C., and E. Gazel (2009), Petrological evidence for secular cooling in mantle plumes, *Nature*, *458*, 619–622, doi:10.1038/nature07857.

Herzberg, C., R. A. Cabral, M. G. Jackson, C. Vidito, J. M. D. Day, and E. H. Hauri (2014), Phantom Archean crust in Mangaia hotspot lavas and the meaning of heterogeneous mantle, *Earth Planet. Sci. Lett.*, *396*, 97–106.

Hirschmann, M. M. (2006), Water, melting, and the deep Earth H_2O cycle, *Annu. Rev. Earth Planet. Sci.*, *34*, 629–653, doi:10.1146/10.1146/annurev.earth.34.031405.125211.

Hirschmann, M. M., T. Tenner, C. Aubaud, and A. C. Withers (2009), Dehydration melting of nominally anhydrous mantle: The primacy of partitioning, *Phys. Earth Planet. Inter.*, *176*, 54–68, doi:10.1016/j.pepi.2009.04.001.

Hirth, G., and D. L. Kohlstedt (1996), Water in the oceanic upper mantle: Implications for rheology, melt extraction and the evolution of the lithosphere, *Earth Planet. Sci. Lett.*, *144*, 93–108.

Hoernle, K., G. Tilton, M. J. Le Bas, S. Duggen, and D. Garbe-Schönberg (2002), Geochemistry of oceanic carbonatites compared with continental carbonatites: Mantle recycling of oceanic crustal carbonate, *Contrib. Mineral. Petrol.*, *142*, 520–542.

Hofmann, A. W. (1997), Mantle geochemistry: The message from oceanic volcanism, *Nature*, *385*, 219–229.

Hofmann, A. W., and S. R. Hart (1978), An assessment of local and regional isotopic equilibrium in the mantle, *Earth Planet. Sci. Lett.*, *38*, 44–62.

Hofmann, A. W., and W. M. White (1982), Mantle plumes from ancient oceanic crust, *Earth Planet. Sci. Lett.*, *57*, 421–436.

Honda, M., and J. D. Woodhead (2005), A primordial solar-neon enriched component in the source of EM-I-type ocean island basalts from the Pitcairn Seamounts, Polynesia, *Earth Planet. Sci. Lett.*, *236*, 597–612, doi:10.1016/j.epsl.2005.05.038.

Jackson, M. G., and R. Dasgupta (2008), Compositions of HIMU, EM1, and EM2 from global trends between radiogenic isotopes and major elements in ocean island basalts, *Earth Planet. Sci. Lett.*, *276*, 175–186, doi:10.1016/j.epsl.2008.09.023.

Jackson, M. G., and A. M. Jellinek (2013), Major and trace element composition of the high ^{3}He/^{4}He mantle: Implications for the composition of a nonchondritic Earth, *Geochem. Geophys. Geosyst.*, *14*, 2954–2976, doi:10.1002/ggge.20188.

Jackson, M. G., S. R. Hart, A. A. P. Koppers, H. Staudigel, J. Konter, J. Blusztajn, M. Kurz, and J. A. Russell (2007), The return of subducted continental crust in Samoan lavas, *Nature*, *448*, 684–687, doi:10.1038/nature06048.

Jackson, M. G., R. W. Carlson, M. D. Kurz, P. D. Kempton, D. Francis, and J. Blusztajn (2010), Evidence for the survival of the oldest terrestrial mantle reservoir, *Nature*, *466*, 853–856, doi:10.1038/nature09287.

Jackson, M. G., D. Weis, and S. Huang (2012), Major element variations in Hawaiian shield lavas: Source features and perspectives from global ocean island basalt (OIB) systematics, *Geochem. Geophys. Geosyst.*, *13*, Q09009, doi:10.1029/2012GC004268.

Jambon, A., B. Déruelle, G. Dreibus, and F. Pineau (1995), Chlorine and bromine abundance in MORB: The contrasting behaviour of the Mid-Atlantic Ridge and East Pacific Rise and implications for chlorine geodynamic cycle, *Chem. Geol.*, *126*, 101–117.

John, T., G. D. Layne, K. M. Haase, and J. D. Barnes (2010), Chlorine isotope evidence for crustal recycling into the Earth's mantle, *Earth Planet. Sci. Lett.*, *298*(1–2), 175–182, doi:10.1016/j.epsl.2010.07.039.

John, T., M. Scambelluri, M. Frische, J. D. Barnes, and W. Bach (2011), Dehydration of subducting serpentinite: Implications for halogen mobility in subduction zones and the deep halogen cycle, *Earth Planet. Sci. Lett.*, *308*(1–2), 65–76, doi:10.1016/j.epsl.2011.05.038.

Kawabata, H., T. Hanyu, Q. Chang, J.-I. Kimura, A. R. L. Nichols, and Y. Tatsumi (2011), The Petrology and geochemistry of St. Helena alkali basalts: Evaluation of the oceanic crust-recycling model for HIMU OIB, *J. Petrol.*, *52*(4), 791–838, doi:10.1093/petrology/egr003.

Kelemen, P. B., G. M. Yogodzinski, and D. W. Scholl (2003), Along-strike variation in lavas of the Aleutian island arc: Implications for the genesis of high Mg# andesite and the continental crust. Inside the Subduction Factory, *Geophys. Monogr. Ser*, *138*, 223–276.

Kelley, K. A., T. Plank, J. Ludden, and H. Staudigel (2003), Composition of altered oceanic crust at ODP Sites 801 and 1149, *Geochem. Geophys. Geosyst.*, *4*(6), 8910, doi:10.1029/2002GC000435.

Kelley, K. A., T. Plank, L. Farr, J. Ludden, and H. Staudigel (2005), Subduction cycling of U, Th, and Pb, *Earth Planet. Sci. Lett.*, *234*, 369–383, doi:10.1016/j.epsl.2005.03.005.

Kelley, K. A., R. Kingsley, and J.-G. Schilling (2013), Composition of plume-influenced mid-ocean ridge lavas and glasses from the Mid-Atlantic Ridge, East Pacific Rise, Galápagos Spreading Center, and Gulf of Aden, *Geochem. Geophys. Geosyst.*, *14*, 223–242, doi:10.1029/2012GC004415.

Kendrick, M. A., R. Arculus, P. Burnard, and M. Honda (2013a), Quantifying brine assimilation by submarine magmas: Examples from the Galápagos Spreading Centre and Lau Basin, *Geochim. Cosmochim. Acta*, *123*, 150–165, doi:10.1016/j.gca.2013.09.012.

Kendrick, M. A., M. Honda, T. Pettke, M. Scambelluri, D. Phillips, and A. Giuliani (2013b), Subduction zone fluxes of halogens and noble gases in seafloor and forearc serpentinites, *Earth Planet. Sci. Lett.*, *365*, 86–96, doi:10.1016/j.epsl.2013.01.006.

Kendrick, M. A., M. G. Jackson, A. J. R. Kent, E. H. Hauri, P. J. Wallace, and J. Woodhead (2014), Contrasting behaviours of CO_2, S, H_2O and halogens (F, Cl, Br, and I) in enriched-mantle melts from Pitcairn and Society seamounts, *Chem. Geol.*, *370*, 69–81, doi:10.1016/j.chemgeo.2014.01.019.

Kent, A. J., M. D. Norman, I. D. Hutcheon, and E. M. Stolper (1999a), Assimilation of seawater-derived components in an oceanic volcano: Evidence from matrix glasses and glass inclusions from Loihi seamount, Hawaii, *Chem. Geol.*, *156*, 299–319.

Kent, A. J., D. A. Clague, M. Honda, E. M. Stolper, I. D. Hutcheon, and M. D. Norman (1999b), Widespread assimilation of a seawater-derived component at Loihi Seamount, Hawaii, *Geochim. Cosmochim. Acta*, *63*, 2749–2761.

Kingsley, R. H. (2002), The geochemistry of basalts from the Easter Microplate boundaries and the Salas y Gomez seamount chain: A comprehensive study of mantle plume-spreading center interaction, dissertation, Univ. of Rhode Island, Narragansett, R. I.

Kingsley, R. H., and J.-G. Schilling (1998), Plume-ridge interaction in the Easter-Salas y Gomez seamount chain-Easter Microplate system: Pb isotope evidence, *J. Geophys. Res.*, *103*, 24,159–24,177.

Kogiso, T., Y. Tatsumi, G. Shimoda, and H. G. Barsczus (1997), High μ (HIMU) ocean island basalts in southern Polynesia: New evidence for whole mantle scale recycling of subducted oceanic crust, *J. Geophys. Res.*, *102*, 8085–8103.

Koleszar, A. M., A. E. Saal, E. H. Hauri, A. N. Nagle, Y. Liang, and M. D. Kurz (2009), The volatile contents of the Galapagos plume: Evidence for H_2O and F open system behavior in melt inclusion, *Earth Planet. Sci. Lett.*, *287*, 442–452, doi:10.1016/j.epsl.2009.08.029.

Krienitz, M.-S., C.-D. Garbe-Schönberg, R. L. Romer, A. Meixner, K. M. Haase, and N. A. Stroncik (2012), Lithium isotope variations in Ocean Island Basalts—Implications for the development of mantle heterogeneity, *J. Petrol.*, *53*(11), 2333–2347, doi:10.1093/petrology/egs052.

Kushiro, I. (1975), On the nature of silicate melt and its significance in magma genesis: Regularities in the shift of the liquidus boundaries involving olivine, pyroxene, and silica minerals, *Am. J. Sci.*, *275*, 411–431.

Langmuir, C., et al. (1997), Hydrothermal vents near a mantle hot spot: The Lucky Strike vent field at 37°N on the Mid-Atlantic Ridge, *Earth Planet. Sci. Lett.*, *148*, 69–91.

Lassiter, J. C., E. H. Hauri, I. K. Nikogosian, and H. G. Barsczus (2002), Chlorine–potassium variations in melt inclusions from Raivavae and Rapa, Austral Islands: Constraints on chlorine recycling in the mantle and evidence for brine-induced melting of oceanic crust, *Earth Planet. Sci. Lett.*, *202*, 525–540.

Lassiter, J. C., J. Blichert-Toft, E. H. Hauri, and H. G. Barsczus (2003), Isotope and trace element variations in lavas from Raivavae and Rapa, Cook-Austral Islands: Constraints on the nature of HIMU- and EM-mantle and the origin of mid-plate volcanism in French Polynesia, *Chem. Geol.*, *202*, 115–138, doi:10.1016/j.chemgeo.2003.08.002.

le Roux, P. J., A. P. le Roex, and J.-G. Schilling (2002), Crystallization processes beneath the southern Mid-Atlantic Ridge (40–55°S), evidence for high-pressure initiation of crystallization, *Contrib. Mineral. Petrol.*, *142*, 582–602.

MacDonald, G. A., and T. Katsura (1965), Eruption of Lassen Peak, Cascade Range, California, in 1915: Example of mixed magmas, *Geol. Soc. Am. Bull.*, *76*, 475–482.

Mackwell, S. J., and D. L. Kohlstedt (1990), Diffusion of hydrogen in olivine: Implications for water in the mantle, *J. Geophys. Res.*, *95*, 5079–5088.

Mallik, A., and R. Dasgupta (2012), Reaction between MORB-eclogite derived melts and fertile peridotite and generation of ocean island basalts, *Earth Planet. Sci. Lett.*, *329–330*, 97–108, doi:10.1016/j.epsl.2012.02.007.

McDonough, W. F., and S. S. Sun (1995), The composition of the Earth, *Chem. Geol.*, *120*, 223–253.

Metrich, N., V. Zanon, L. Creon, A. Hildenbrand, M. Moreira, and F. O. Marques (2014), Is the ''Azores Hotspot'' a Wetspot? Insights from the Geochemistry of Fluid and Melt Inclusions in Olivine of Pico Basalts, *J. Petrol.*, *55*(2), 377–393, doi:10.1093/petrology/egt071.

Michael, P. (1995), Regionally distinctive sources of depleted MORB: Evidence from trace elements and H_2O, *Earth Planet. Sci. Lett.*, *131*, 301–320.

Michael, P. J., and W. C. Cornell (1998), Influence of spreading rate and magma supply on crystallization and assimilation beneath mid-ocean ridges: Evidence from chlorine and major element chemistry of mid-ocean ridge basalts, *J. Geophys. Res.*, *103*, 18,325–18,356.

Michael, P. J., and J.-G. Schilling (1989), Chlorine in mid-ocean ridge magmas: Evidence for assimilation of seawater-influenced components, *Geochim. Cosmochim. Acta*, *53*, 3131–3143.

Nakamura, Y., and M. Tatsumoto (1988), Pb, Nd, and Sr isotopic evidence for a multicomponent source for rocks of Cook-Austral Islands and heterogeneities of mantle plumes, *Geochim. Cosmochim. Acta*, *52*, 2909–2924.

Nishio, Y., S. Nakai, T. Kogiso, and H. Barsczus (2005), Lithium, strontium, and neodymium isotopic compositions of oceanic island basalts in the Polynesian region: Constraints on a Polynesian HIMU origin, *Geochem. J.*, *39*, 91–103.

O'Leary, J. A., G. A. Gaetani, and E. H. Hauri (2010), The effect of tetrahedral Al^{3+} on the partitioning of water between clinopyroxene and silicate melt, *Earth Planet. Sci. Lett.*, *297*(1–2), 111–120, doi:10.1016/j.epsl.2010.06.011.

Pan, Y., and R. Batiza (1998), Major element chemistry of volcanic glasses from the Easter Seamount Chain: Constraints on melting conditions in the plume channel, *J. Geophys. Res.*, *103*, 5287–5304.

Parai, R., S. Mukhopadhyay, and J. C. Lassiter (2009), New constraints on the HIMU mantle from neon and helium isotopic compositions of basalts from the Cook-Austral Islands, *Earth Planet. Sci. Lett.*, *277*(1–2), 253–261, doi:10.1016/j.epsl.2008.10.014.

Paul, B., J. D. Woodhead, J. Hergt, L. Danyushevsky, T. Kunihiro, and E. Nakamura (2011), Melt inclusion Pb-isotope analysis by LA-MC-ICPMS: Assessment of analytical performance and application to OIB genesis, *Chem. Geol.*, *289*, 210–223, doi:10.1016/j.chemgeo.2011.08.005.

Portnyagin, M., K. Hoernle, P. Plechov, N. Mironov, and S. Khubunaya (2007), Constraints on mantle melting and composition and nature of slab components in volcanic arcs from volatiles (H_2O, S, Cl, F) and trace elements in melt inclusions from the Kamchatka Arc, *Earth Planet. Sci. Lett.*, *255*, 53–69, doi:10.1016/j.epsl.2006.12.005.

Rose-Koga, E. F., K. T. Koga, P. Schiano, M. Le Voyer, N. Shimizu, M. J. Whitehouse, and R. Clocchiatti (2012), Mantle source heterogeneity for South Tyrrhenian magmas revealed by Pb isotopes and halogen contents of olivine-hosted melt inclusions, *Chem. Geol.*, *334*, 266–279, doi:10.1016/j.chemgeo.2012.10.033.

Rose-Koga, E. F., K. T. Koga, M. Hamada, T. Hélouis, M. J. Whitehouse, and N. Shimizu (2014), Volatile (F and Cl) concentrations in Iwate olivine-hosted melt inclusions indicating low-temperature subduction, *Earth Planets Space*, *66*, 81.

Roy-Barman, M., and C. J. Allègre (1995), $^{187}Os/^{186}Os$ in oceanic island basalts: Tracing oceanic crust recycling in the mantle, *Earth Planet. Sci. Lett.*, *129*, 145–161.

Saal, A. E., S. R. Hart, N. Shimizu, E. H. Hauri, and G. D. Layne (1998), Pb isotopic variability in melt inclusions from Oceanic Island Basalts, Polynesia, *Science*, *282*, 1481–1484, doi:10.1126/science.282.5393.1481.

Saal, A. E., E. H. Hauri, C. H. Langmuir, and M. R. Perfit (2002), Vapour undersaturation in primitive mid-ocean-ridge basalt and the volatile content of Earth's upper mantle, *Nature*, *419*, 451–455.

Saal, A. E., S. R. Hart, N. Shimizu, E. H. Hauri, G. D. Layne, and J. M. Eiler (2005), Pb isotopic variability in melt inclusions from the EMI-EMII-HIMU mantle end-members and the role of the oceanic lithosphere, *Earth Planet. Sci. Lett.*, *240*, 605–620, doi:10.1016/j.epsl.2005.10.002.

Salters, V., and W., White (1998), Hf isotope constraints on mantle evolution, *Chem. Geol.*, *145*, 447–460.

Salters, V. J. M., and A. Sachi-Kocher (2010), An ancient metasomatic source for the Walvis Ridge basalts, *Chem. Geol.*, *273*, 151–167, doi: 10.1016/j.chemgeo.2010.02.010.

Salters, V. J. M., and A. Stracke (2004), Composition of the depleted mantle, *Geochem. Geophys. Geosyst.*, *5*, Q05004, doi:10.1029/2003GC000597.

Salters, V. J. M., S. Mallick, S. R. Hart, C. E. Langmuir, and A. Stracke (2011), Domains of depleted mantle: New evidence from hafnium and neodymium isotopes, *Geochem. Geophys. Geosyst.*, *12*, Q08001, doi:10.1029/2011GC003617.

Sarbas, B. (2008), The GEOROC database as part of a growing geoinformatics network, translated by S. R. Brady, A. K. Sinha, and L. C. Gundersen, Geoinformatics. Data to Knowledge, Proceedings, *U. S. Geol. Surv. Sci. Invest. Rep.*, pp. 42–43.

Schiano, P., K. W. Burton, B. Dupré, J.-L. Birck, G. Guille, and C. J. Allègre (2001), Correlated Os-Pb-Nd-Sr isotopes in the Austral-Cook chain basalts: The nature of mantle components in plume sources, *Earth Planet. Sci. Lett.*, *186*, 527–537.

Schilling, J.-G., H. Sigurdsson, A. N. Davis, and R. N. Hey (1985), Easter microplate evolution, *Nature*, *317*, 325–331.

Shaw, A. M., M. D. Behn, S. E. Humphris, R. A. Sohn, and P. M. Gregg (2010), Deep pooling of low degree melts and volatile fluxes at the 85°E segment of the Gakkel Ridge: Evidence from olivine-hosted melt inclusions and glasses, *Earth Planet. Sci. Lett.*, *289*(3–4), 311–322, doi:10.1016/j.epsl.2009.11.018.

Simons, K., J. Dixon, J.-G. Schilling, R. Kingsley, and R. Poreda (2002), Volatiles in basaltic glasses from the Easter-Salas y Gomez Seamount Chain and Easter Microplate: Implications for geochemical cycling of volatile elements, *Geochem. Geophys. Geosyst.*, *3*, 1–29, doi: 10.1029/2001GC000173.

Smith, J. V. (1981), Halogen and phosphorus storage in the Earth, *Nature*, *289*, 762–765.

Smith, J. V., J. S. Delaney, R. L. Hervig, and J. B. Dawson (1981), Storage of F and Cl in the upper mantle: Geochemical implications, *Lithos*, *14*, 133–147.

Sobolev, A. V., and L. V. Danyushevsky (1994), Petrology and geochemistry of boninites from the north termination of the Tonga Trench: Constraints on the generation conditions of primary high-carboninite magmas, *J. Petrol.*, *35*, 1183–1211.

Spilliaert, N., N. Métrich, and P. Allard (2006), S-Cl-F degassing pattern of water-rich alkali basalt: Modelling and relationship with eruption styles on Mount Etna volcano, *Earth Planet. Sci. Lett.*, *248*, 772–786, doi:10.1016/j.epsl.2006.06.031.

Staudigel, H., A. Zindler, S. Hart, and T. Leslie (1984), The isotope systematics of a juvenile intraplate volcano: Pb, Nd, and Sr isotope ratios of basalts from Loihi Seamount, Hawaii, *Earth Planet. Sci. Lett.*, *69*, 13–29.

Staudigel, H., T. Plank, B. White, and H. Schmincke (1996), Geochemical fluxes during seafloor alteration of the basaltic upper oceanic crust: DSDP Sites 417 and 418: Subduction: Top to Bottom, *Geophys. Monogr.*, *96*, 19–38.

Stracke, A., M. Bizimis, and V. J. M. Salters (2003), Recycling oceanic crust: Quantitative constraints, *Geochem. Geophys. Geosyst.*, *4*(3), 8003, doi:10.1029/2001GC000223.

Straub, S. M., and G. D. Layne (2003), The systematics of chlorine, fluorine, and water in Izu arc front volcanic rocks: Implications for volatile recycling in subduction zones, *Geochim. Cosmochim. Acta*, *67*(21), 4179–4203, doi:10.1016/S0016-7037(03)00307-7.

Stroncik, N. A., and K. M. Haase (2004), Chlorine in oceanic intraplate basalts: Constraints on mantle sources and recycling processes, *Geology*, *32*(11), 945, doi:10.1130/G21027.1.

Tatsumi, Y., K. Oguri, G. Shimoda, T. Kogiso, and H. G. Barsczus (2000), Contrasting behavior of noble-metal elements during magmatic differentiation in basalts from the Cook Islands, Polynesia, *Geology*, *28*, 131–134.

van Keken, P. E., B. R. Hacker, E. M. Syracuse, and G. A. Abers (2011), Subduction factory. 4: Depth-dependent flux of H_2O from subducting slabs worldwide, *J. Geophys. Res.*, *116*, B01401, doi:10.1029/2010JB007922.

Van Orman, J. A., T. L. Grove, and N. Shimizu (2001), Rare earth element diffusion in diopside: Influence of temperature, pressure, and ionic radius, and an elastic model for diffusion in silicates, *Contrib. Mineral. Petrol.*, *141*, 687–703, doi:10.1007/s004100100269.

Wallmann, K. (2001), The geological water cycle and the evolution of marine $\delta^{18}O$ values, *Geochim. Cosmochim. Acta*, *65*, 2469–2485.

Weaver, B. L. (1991), The origin of ocean island basalt end-member compositions: Trace element and isotopic constraints, *Earth Planet. Sci. Lett.*, *104*, 381–397.

White, W. M. (2010), Oceanic Island Basalts and mantle plumes: The geochemical perspective, *Annu. Rev. Earth Planet. Sci.*, *38*, 133–160, doi: 10.1146/annurev-earth-040809-152450.

White, W. M., and A. W. Hofmann (1982), Sr and Nd isotope geochemistry of oceanic basalts and mantle evolution, *Nature*, *296*, 821–825.

Witham, F., J. Blundy, S. C. Kohn, P. Lesne, J. Dixon, S. V. Churakov, and R. Botcharnikov (2012), SolEx: A model for mixed COHSCl-volatile solubilities and exsolved gas compositions in basalt, *Comput. Geosci.*, *45*, 87–97, doi:10.1016/j.cageo.2011.09.021.

Woodhead, J. D. (1996), Extreme HIMU in an oceanic setting: The geochemistry of Mangaia Island (Polynesia), and temporal evolution of the Cook-Austral hotspot, *J. Volcanol. Geotherm. Res.*, *72*, 1–19.

Woodhead, J. D., and C. W. Devey (1993), Geochemistry of the Pitcairn seamounts. I: Source character and temporal trends, *Earth Planet. Sci. Lett.*, *116*, 81–99.

Workman, R. K., S. R. Hart, M. Jackson, M. Regelous, K. A. Farley, J. Blusztajn, M. Kurz, and H. Staudigel (2004), Recycled metasomatized lithosphere as the origin of the Enriched Mantle II (EM2) end-member: Evidence from the Samoan Volcanic Chain, *Geochem. Geophys. Geosyst.*, *5*, Q04008, doi:10.1029/2003GC000623.

Workman, R. K., E. Hauri, S. R. Hart, J. Wang, and J. Blusztajn (2006), Volatile and trace elements in basaltic glasses from Samoa: Implications for water distribution in the mantle, *Earth Planet. Sci. Lett.*, *241*, 932–951, doi:10.1016/j.epsl.2005.10.028.

Wu, J., and K. T. Koga (2013), Fluorine partitioning between hydrous minerals and aqueous fluid at 1GPa and 770–947°C: A new constraint on slab flux, *Geochim. Cosmochim. Acta*, *119*, 77–92, doi:10.1016/j.gca.2013.05.025.

Yang, H.-J., F. A. Frey, and D. A. Clague (2003), Constraints on the source components of lavas forming the Hawaiian North Arch and Honolulu Volcanics, *J. Petrol.*, *44*, 603–627.

Yurimoto, H., T. Kogiso, K. Abe, H. G. Barsczus, A. Utsunomiya, and S. Maruyama (2004), Lead isotopic compositions in olivine-hosted melt inclusions from HIMU basalts and possible link to sulfide components, *Phys. Earth Planet. Inter.*, *146*, 231–242, doi:10.1016/j.pepi.2003.08.013.

Zhang, Y. (2008), *Geochemical Kinetics*, pp. 173–324, Princeton Univ. Press, Princeton, N. J.

Zindler, A., and S. Hart (1986), Chemical geodynamics, *Annu. Rev. Earth Planet. Sci.*, *14*, 493–571.

Zindler, A., E. Jagoutz, and S. Goldstein (1982), Nd, Sr and Pb isotopic systematics in a three-component mantle: A new perspective, *Nature*, *298*, 519–523.